

Long-range PM_{2.5} pollution and health impacts from the 2023 Canadian wildfires

<https://doi.org/10.1038/s41586-025-09482-1>

Received: 31 March 2024

Accepted: 31 July 2025

Published online: 10 September 2025

Open access

 Check for updates

Qiang Zhang^{1,9}, Yuexuanzi Wang^{1,9}, Qingyang Xiao^{2,9}, Guannan Geng², Steven J. Davis³, Xiaodong Liu², Jin Yang¹, Jiajun Liu², Wenyu Huang¹, Changpei He¹, Binhe Luo⁴, Randall V. Martin⁵, Michael Brauer^{6,7}, James T. Randerson⁸ & Kebin He²

Smoke from extreme wildfires in Canada adversely affected air quality in many regions in 2023^{1,2}. Here we use satellite observations, machine learning and a chemical transport model to quantify global and regional PM_{2.5} (particulate matter less than 2.5 µm in diameter) exposure and human health impacts related to the 2023 Canadian wildfires. We find that the fires increased annual PM_{2.5} exposure worldwide by 0.17 µg m⁻³ (95% confidence interval, 0.09–0.26 µg m⁻³). North America had the largest increase in annual mean exposure (1.08 µg m⁻³; 0.82–1.34 µg m⁻³), but there were also increases in Europe (0.41 µg m⁻³; 0.32–0.50 µg m⁻³) owing to long-range transport. Annual mean PM_{2.5} exposure in Canada increased by 3.82 µg m⁻³ (3.00–4.64 µg m⁻³). In the USA, the contribution of the Canadian fires to increased PM_{2.5} was 1.49 µg m⁻³ (1.22–1.77 µg m⁻³), four times as large as the contribution from the 2023 wildfires originating in the USA. We find that 354 million (277–421 million) people in North America and Europe were exposed to daily PM_{2.5} air pollution caused by Canadian wildfires in 2023. We estimate that 5,400 (3,400–7,400) acute deaths in North America and 64,300 (37,800–90,900) chronic deaths in North America and Europe were attributable to PM_{2.5} exposure to the 2023 Canadian wildfires. Our results highlight the far-reaching PM_{2.5} pollution and health burden that large wildfires can have in a single year.

Wildfires impact the global carbon cycle^{3,4}, ecosystems^{5,6}, air quality^{7–11} and human health^{12–15}. Among these impacts, the contribution of wildfires to global PM_{2.5} pollution has been steadily increasing in recent years, with the largest increase in North America^{8–11}. Between May and September of 2023, severe wildfires in Canada burned a total of 15 million ha of forest (about 4% of the total forest area in Canada and more than 7 times the annual mean burned area for 1983–2022) and resulted in vast carbon emissions (647 TgC)^{16,17}. Smoke generated from the Canadian wildfires was not only transported across North America and led to air-quality alerts in many regions of the USA¹ but also transported across the North Atlantic to reach Europe and Asia², which underscored that severe wildfires do not have only local consequences. Although PM_{2.5} exposure from wildfires has been investigated in different ways^{8–11,18–20} and transboundary fire pollution episodes have been identified in previous studies^{21–29}, the impacts of such extreme wildfires on global air quality and human health remain underexplored^{30–32}. Given the potential continued impact from projected increase in future wildfires^{33–35}, quantifying exposure to this air pollution and the level of health impact at a global extent can inform responses, including fire monitoring and forecasting, fire suppression, land management and landscape-scale fuel treatments, and climate mitigation more broadly.

Here we combine several global models and observation datasets to develop a near-real-time framework to estimate global and regional PM_{2.5} exposure (that is, population-weighted mean PM_{2.5} concentration) and deaths attributable to the 2023 Canadian wildfires (Extended Data Fig. 1). Details of our analytic approach are in Methods. In summary, we first use the GEOS-Chem chemical transport model (a global three-dimensional model of atmospheric chemistry driven by meteorological input from the Goddard Earth Observing System)³⁶ and three near-real-time global fire emission inventories (the Global Fire Emissions Database (GFED)³⁷, the Quick Fire Emissions Dataset (QFED)³⁸ and the Global Fire Assimilation System (GFAS)³⁹) to derive global daily PM_{2.5} concentrations and the fractional share of these concentrations related to wildfires. We then use a machine-learning approach to retrieve the global daily PM_{2.5} concentration from a range of data, including ground-monitoring measurements, satellite retrievals, reanalysis data and GEOS-Chem model simulations (Supplementary Fig. 1), and attribute the share of retrieved total PM_{2.5} concentration to wildfires using the previously simulated fractional contribution. By performing a series of evaluation and sensitivity tests to the three inventories (Supplementary Table 1), the results presented hereafter correspond to estimates with the GFED as a priori input and the impacts of using different inventories on our conclusions are discussed ('Discussion').

¹Ministry of Education Key Laboratory for Earth System Modeling, Department of Earth System Science, Tsinghua University, Beijing, China. ²State Key Joint Laboratory of Environmental Simulation and Pollution Control, School of Environment, Tsinghua University, Beijing, China. ³Department of Earth System Science, Stanford University, Stanford, CA, USA. ⁴State Key Laboratory of Earth Surface Processes and Disaster Risk Reduction, Beijing Normal University, Beijing, China. ⁵Department of Energy, Environmental, and Chemical Engineering, Washington University in St. Louis, St. Louis, MO, USA. ⁶School of Population and Public Health, University of British Columbia, Vancouver, British Columbia, Canada. ⁷Institute for Health Metrics and Evaluation, University of Washington, Seattle, WA, USA. ⁸Department of Earth System Science, University of California, Irvine, Irvine, CA, USA. ⁹These authors contributed equally: Qiang Zhang, Yuexuanzi Wang, Qingyang Xiao. ✉e-mail: qiangzhang@tsinghua.edu.cn

We further attribute fire-related PM_{2.5} concentrations to wildfires in different source regions (that is, Eastern Canada, Western Canada, Western USA, Eastern USA and other global regions) by using a zero-out approach with the GFED inventory (Supplementary Table 2). Finally, we use previously established exposure–response functions^{15,40} to estimate acute and chronic deaths attributable to PM_{2.5} exposure from Canadian wildfires. It should be noted that various exposure–response functions are available and that the mortality estimates are highly dependent on the function used (‘Discussion’). Unless otherwise specified, ranges of results reported reflect the 95% confidence interval (CI) and numbers of deaths reported reflect the median rounded to the nearest hundred.

Primary emissions of carbon dioxide (CO₂) and air pollutants from the 2023 Canadian wildfires are substantially different in three bottom-up fire emission inventories (that is, GFED, QFED and GFAS), ranging from 139 TgC to 658 TgC, from 0.55 Tg to 0.76 Tg black carbon, and from 8.9 Tg to 15.0 Tg organic carbon (Extended Data Fig. 2a). Despite differences in the magnitude of emissions, there is consensus among the three bottom-up inventories that the 2023 Canadian fire emissions were the highest in at least 20 years. Emissions of CO₂ and primary aerosols in 2023 were 4.9–10.7-times higher than the annual average for 2003–2022 and 2.9–5.1-times higher than in 2021 (the year with the next highest emissions; Extended Data Fig. 2b).

Transboundary smoke exposure

We estimate that wildfires worldwide accounted for a global annual mean PM_{2.5} exposure of 1.32 µg m⁻³ (95% CI, 0.66–1.98 µg m⁻³) in 2023. Of this total, the Canadian fires account for 0.17 µg PM_{2.5} m⁻³ (95% CI, 0.09–0.26 µg PM_{2.5} m⁻³), or 13% of the total fire-related PM_{2.5} exposure. Despite this relatively small global impact, PM_{2.5} smoke from Canadian fires spread across the North American continent and was transported to Europe (Fig. 1a; global region definition presented in Extended Data Fig. 3a). Indeed, the Canadian fires account for more than half of fire-related PM_{2.5} exposure along the western coasts of Europe (Fig. 1e,h), and increased annual mean PM_{2.5} exposure of 1.08 µg m⁻³ (95% CI, 0.82–1.34 µg m⁻³) and 0.41 µg m⁻³ (95% CI, 0.32–0.50 µg m⁻³) in North America and Europe, respectively (Extended Data Table 1). In Europe, 90% of the total population (620 million) were exposed to more than 0.32 µg m⁻³ of increased annual mean PM_{2.5} concentrations owing to the 2023 Canadian wildfires. The contribution of the 2023 Canadian wildfires to the annual mean PM_{2.5} exposure in other world regions was comparatively small and statistically insignificant when compared with the interannual variability (Methods).

Nearer to and directly downwind of the wildfires, impacts were much more substantial. Because wildfires in the USA and elsewhere affected PM_{2.5} pollution at the same time as the Canadian fires, we separately analyse PM_{2.5} exposure in Canada and the USA related to fire emissions from five different regions: Eastern Canada, Western Canada, the Eastern USA, the Western USA and fires in all other regions (see source region definitions and the Environmental Protection Agency’s delineation of North American ecological regions in Extended Data Fig. 3b and Supplementary Fig. 2).

Extended Data Fig. 4 shows the annual mean PM_{2.5} concentrations in Canada and the USA that are related to the fires in each country. Although smoke from US fires affected pollution concentrations along the southern boundary of Western Canada, fire-related PM_{2.5} across Canada as a whole was dominated by its own fires. Annual mean PM_{2.5} exposure in Canada itself increased by 3.82 µg m⁻³ (95% CI, 3.00–4.64 µg m⁻³) owing to its own fires (maximum monthly mean exposure of 16.07 µg m⁻³ in June; Extended Data Fig. 5). PM_{2.5} hotspots in Canada include the James Bay region of Quebec and large areas of Alberta, Saskatchewan and the Northwest Territories (Extended Data Fig. 4a), which is consistent with the distribution of burned area and sources of primary emissions (Extended Data Fig. 6). Although wildfires in Western Canada and Eastern Canada had comparable impacts on PM_{2.5}

concentrations in Eastern Canada, the wildfires in Eastern Canada had only a small effect on pollution in Western Canada (Fig. 2; see impacted region definitions in Extended Data Fig. 3c).

In the USA, the 2023 Canadian fires accounted for 1.49 µg m⁻³ (95% CI, 1.22–1.77 µg m⁻³) of the annual mean PM_{2.5} exposure (maximum monthly mean exposure of 8.04 µg m⁻³ in June; Extended Data Fig. 5), which is four times as large as the 0.35 µg m⁻³ (95% CI, 0.29–0.42 µg m⁻³) exposure related to fires in the USA in the same year. As shown in Extended Data Fig. 4c, PM_{2.5} concentrations in the USA were impacted by smoke plumes from Canada that extended over large areas of the Rocky Mountains, the Midwest, Ohio Valley and the Northeast regions. The US Midwest was especially affected: the annual mean PM_{2.5} exposure in the region increased by 3.13 µg m⁻³ (95% CI, 2.82–3.44 µg m⁻³; Fig. 2). In comparison, the annual mean PM_{2.5} exposures increased by 2.35 µg m⁻³ (95% CI, 2.11–2.59 µg m⁻³) in Ohio Valley, 2.52 µg m⁻³ (95% CI, 2.27–2.78 µg m⁻³) in the Northeast, and 1.92 µg m⁻³ (95% CI, 1.69–2.15 µg m⁻³) in the Rocky Mountains. At the state level, the largest PM_{2.5} impacts were in North Dakota (3.85 µg m⁻³; 95% CI, 3.39–4.31 µg m⁻³). Meanwhile, the impacts of the Canadian fires on the Southwest and West regions of the USA were modest. Nonetheless, in 7 of the 9 regions of the continental USA analysed, the Canadian fires increased the annual PM_{2.5} exposure by more than 0.5 µg m⁻³, and increased the annual PM_{2.5} exposure by more than 1 µg m⁻³ for 187 million Americans (57% of total; Extended Data Fig. 7). As in Canada, the downwind effects of the 2023 fires in Western Canada affected US air quality more than the fires in Eastern Canada: 60% of the annual exposure in the USA related to Canadian fires was from Western Canada.

Figure 3 shows the daily and cumulative PM_{2.5} exposure in Canada, the USA and Europe related to different sources of fire emissions. In Canada, there were frequent large spikes of air pollution throughout the spring, summer and autumn of 2023 related in particular to persistent fires in Western Canada (Fig. 3a). The magnitude of pollution episodes was mostly lower in the USA, but fires in Eastern Canada caused two spikes in June that led to the national daily average PM_{2.5} exposure exceeding 30 µg m⁻³ (Fig. 3b and Supplementary Table 3). During these two episodes, a low-pressure system over the Canadian Maritime Provinces coupled with a high-pressure ridge to the west channelled a plume of pollution into population centres of the Eastern USA (Supplementary Figs. 3–5). In contrast, wildfires in Western Canada had a persistent and overall larger impact on US air quality throughout the fire season (Fig. 3e). Smoke from these western fires was transported eastwards along the northern margin of the Rocky Mountains and then spread first south-eastwards into the Great Plains and then back up into the northeast owing to the greatly developed subpolar low pressure (Supplementary Fig. 6).

As shown in Fig. 1d, the 2023 Canadian fires also had broad impacts on PM_{2.5} exposure in Western Europe, especially in Mediterranean countries such as Spain, Italy and France (also see Methods and Supplementary Figs. 7–12). The smoke plumes from Canada were transmitted eastwards into Europe by a westerly airflow situated over the mid-latitudes and crossed the North Atlantic (Supplementary Fig. 7). The largest episodes of trans-Atlantic pollution occurred in late June owing to the large polewards pressure gradient between the Azores high and the Icelandic low, leading to widespread air pollution in Europe (Supplementary Fig. 8). As in the USA, though, the Western Canadian fires led to greater cumulative exposure in Europe (Fig. 3f).

Health impacts

We further quantify the extent of the Canadian fires’ impacts on global health by the number of ‘Canada smoke days’ in which both (1) the daily mean PM_{2.5} concentrations exceeded 15 µg m⁻³ (the recommended 24-hour guideline levels of the World Health Organization (WHO)) and (2) the Canadian fires accounted for at least 50% of the total 24-hour average PM_{2.5} concentration. With these criteria, 354 million (95% CI, 277–421 million) people in North America and Europe were exposed

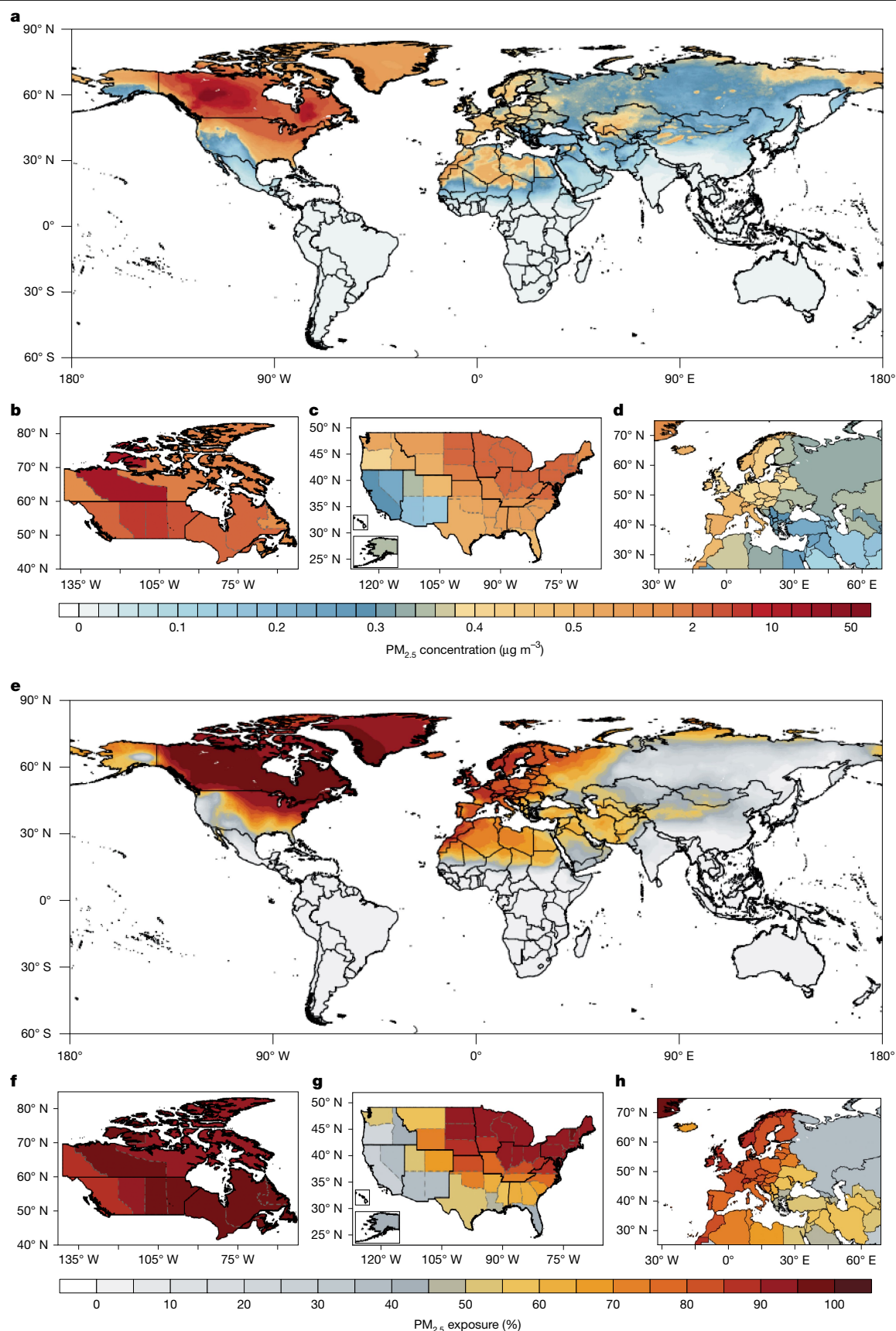


Fig. 1 | Global and regional $PM_{2.5}$ pollution from the 2023 Canadian wildfires.

a, Global annual mean $PM_{2.5}$ concentrations from Canadian fires in 2023. **b–d**, Regional annual mean $PM_{2.5}$ exposure (population-weighted mean) in Canada (**b**), the USA (**c**) and Europe (**d**) from Canadian fires in 2023. **e**, Global

fraction of annual mean $PM_{2.5}$ concentration from the 2023 Canadian fires in total fire-related $PM_{2.5}$ concentration. **f–h**, Regional fraction of annual mean $PM_{2.5}$ exposure in Canada (**f**), the USA (**g**) and Europe (**h**) from the 2023 Canadian fires in total fire-related $PM_{2.5}$ exposure.

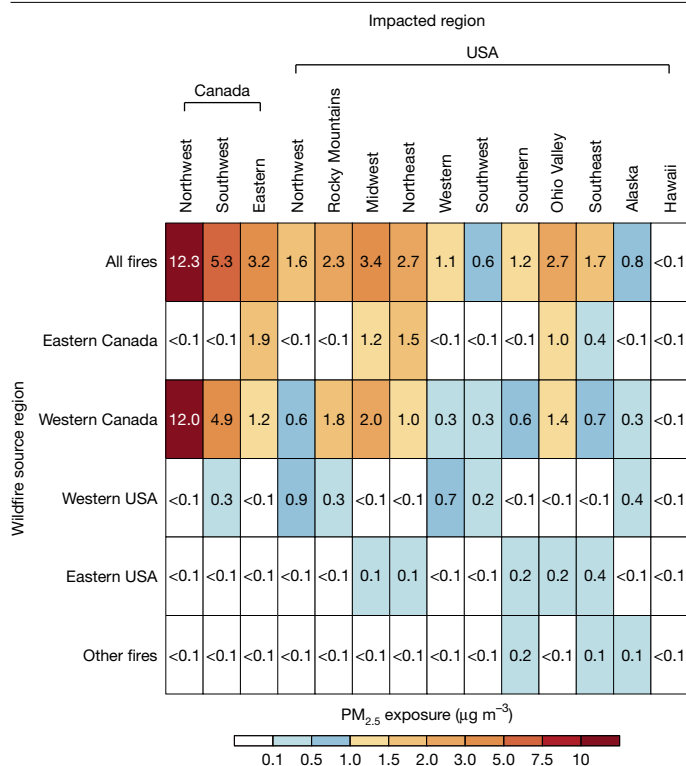


Fig. 2 | The 2023 annual mean PM_{2.5} exposure in Canada and the USA owing to fires from different source regions. Each cell in the grid shows population-weighted mean PM_{2.5} concentrations in each impacted region of Canada and the USA (indicated by the column) by fire source regions (indicated by the row). The definition of wildfire source regions in Canada and the USA are presented in Extended Data Fig. 3b, and the impacted regions are defined in Extended Data Fig. 3c. 'Other fires' means fires from other global regions apart from Canada and the USA.

to at least 1 Canada smoke days in 2023, with a total of 4.84 billion person-days of exposure in that year (Extended Data Table 1). In the USA alone, 267 million (95% CI, 222–273 million) people (79% of total) were exposed to at least 1 Canada smoke days—3.69 billion person-days of exposure. In addition, 98% of the Canadian population (38.1 million people; 95% CI, 37.0–38.1 million) experienced such Canada smoke days, with an average of 27.1 days per person. Although the annual mean PM_{2.5} exposure from Canadian fires was larger in Canada than in the USA, total person-days exposure to Canada smoke days was three-times greater in the USA owing to the much larger population in downwind areas of the USA. Similarly, 47.7 million (95% CI, 17.0–104.7 million) people in Europe were exposed to Canada smoke days (more people than in Canada itself), with an average of 1.0 days per person, mostly during the period between 26 June and 7 July. In turn, we estimate 5,400 (95% CI, 3,400–7,400) acute deaths attributable to exposure on those Canada smoke days, including 4,100 (95% CI, 2,600–5,600) in the USA and 1,300 (95% CI, 800–1,800) in Canada (Fig. 4a).

With 5 months of continuous exposure to smoke from the 2023 Canadian wildfires (Fig. 3), the chronic health impacts of the 2023 Canadian wildfires were also substantial and widespread (Fig. 4b). Worldwide, we estimate that 82,100 (95% CI, 47,700–116,500) people died prematurely attributable to chronic smoke exposure from the 2023 Canadian wildfires (or 0.9% of the total PM_{2.5}-related deaths and 0.1% of total all-cause deaths worldwide in 2023), with 64,300 (95% CI, 37,800–90,900) deaths occurring in North America and Europe. Of these deaths, 41,900 (95% CI, 28,400–55,400) occurred in North America, including 33,000 (95% CI, 22,500–43,500) in the USA and 8,300 (95% CI, 5,800–10,800) in Canada (accounting for about 17% and 39% of total PM_{2.5} attributable deaths or 1.2% and 2.9% of total all-cause deaths in those countries in 2023,

respectively). Longer-range health impacts were also substantial. In Europe, we estimate 22,400 (95% CI, 14,900–29,900) attributable chronic deaths in Europe related to the intercontinental transport of smoke from the Canadian fires (Fig. 4b), accounting for 3.8% of total PM_{2.5} attributable deaths and 0.3% of total all-cause deaths in 2023.

Discussion

Our results quantify the magnitude and extent of smoke pollution and health impacts related to the 2023 Canadian wildfires. Although our analysis is focused on the year 2023, we also compare the results with 2021 and 2017, which had the second- and third-greatest wildfire emissions from Canada since 2000 (Extended Data Fig. 2b). The 2023 Canadian wildfires induced 2.6-times and 5.3-times higher global annual PM_{2.5} exposure than that of 2021 and 2017, respectively, demonstrating the large impacts on global air pollution. Previous studies have argued that wildfire-related PM_{2.5} has influenced trends in annual PM_{2.5} concentration in the USA since 2016⁹. With increasing PM_{2.5} exposure from Canadian wildfires from 2017 to 2023 (2017, 0.26 µg m⁻³; 2021, 0.55 µg m⁻³; 2023, 1.49 µg m⁻³), our results show that transboundary smoke pollution may have remarkably contributed to the reversed PM_{2.5} trend in the USA.

Our model can be evaluated in multiple ways. First, the station-based 20-fold cross-validation shows that the global daily PM_{2.5} concentrations we model agree well with surface observations ($R^2 = 0.84$, root-mean-squared error (RMSE) = 8.62 µg m⁻³; Extended Data Fig. 8) and are comparable to other recent studies^{10,41}. Second, following a similar approach to ref. 10, modelled daily PM_{2.5} concentrations are compared with surface observations during fire events in Canada and the USA (Methods). During 20 such fire events in Canada and the USA (which together account for >80% of fire-related PM_{2.5} exposure in 2023), our results agree well with daily PM_{2.5} observations in both Canada ($R^2 = 0.59$, RMSE = 16.50 µg m⁻³) and the USA ($R^2 = 0.78$, RMSE = 12.50 µg m⁻³) (Extended Data Fig. 9 and Supplementary Table 4).

More importantly, to investigate the impact of different emission estimates in fire inventories^{42,43}, we conduct two additional sensitivity analyses to derive global daily PM_{2.5} concentrations by using the QFED and the GFAS as the a priori inventory. In general, we found that the performances of the three inventories are comparable. Machine-learning-based global daily PM_{2.5} concentrations with the three fire inventories (that is, GFED, QFED and GFAS) show similar accuracy when comparing with surface observations in the sample-based cross-validation ($R^2 = 0.87$ – 0.88 , RMSE = 7.46–7.92 µg m⁻³; Supplementary Fig. 13 and Supplementary Tables 5 and 6). During 20 selected fire events, modelled daily PM_{2.5} concentrations with the different fire inventories show consistent performance against surface observations in the USA ($R^2 = 0.78$ – 0.80 , RMSE = 11.70–12.50 µg m⁻³) but moderate differences in Canada ($R^2 = 0.59$ – 0.75 , RMSE = 12.83–16.50 µg m⁻³). Global fire-related annual PM_{2.5} exposure in 2023 estimated with the GFED and the GFAS are very close (1.32 µg m⁻³ and 1.30 µg m⁻³, respectively), whereas the QFED-based estimates (2.36 µg m⁻³) are 79% higher than the other two. In Canada, fire-related annual PM_{2.5} exposure estimated with the 3 inventories shows better agreement (3.75–4.49 µg m⁻³) than the global average. In the USA, GFED- and GFAS-based estimates on fire-related annual PM_{2.5} exposure in 2023 are close to each other, whereas the QFED-based estimates are 59–70% higher, as does the comparison with other recent studies (Supplementary Fig. 14). To put our results in context with recent analyses using a similar approach^{9–11,44}, we present the GFED-based estimates in this work, and we believe that the impacts of fire inventory choice on our conclusions are minor given their similar fire-related PM_{2.5} exposure estimates in Canada.

Various exposure–response functions have been used in previous studies (Supplementary Tables 7–9) when estimating acute and chronic deaths attributable to wildfire PM_{2.5} exposure, including functions derived from global^{15,40,45,46} or regional^{47–49} meta-analysis and derived

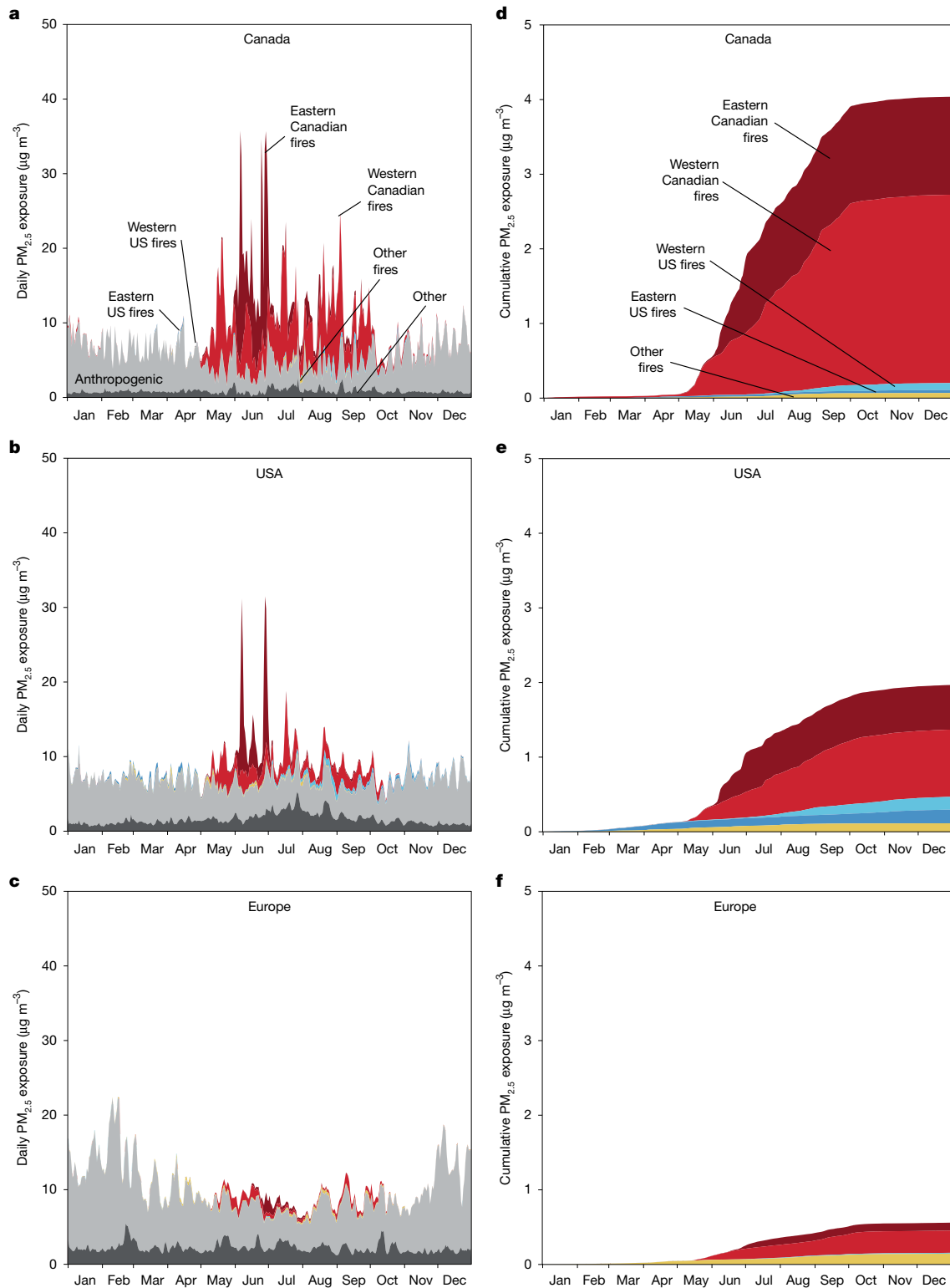


Fig. 3 | Daily and cumulative $\text{PM}_{2.5}$ exposures from different sources in 2023. **a–c**, Daily $\text{PM}_{2.5}$ exposure in Canada (**a**), the USA (**b**) and Europe (**c**) from fire sources in different source regions, anthropogenic sources and other sources (for example, biogenic, dust and sea salt). **d–f**, Cumulative fire-related $\text{PM}_{2.5}$

exposures in Canada (**d**), the USA (**e**) and Europe (**f**) from different source regions. The definitions of wildfire source regions in Canada and the USA are presented in Extended Data Fig. 3b. ‘Other fires’ means fires from other global regions apart from Canada and the USA.

for all-cause mortality^{15,40,46–50} or cause-specific mortality⁴⁵. Here we use widely used global pooled functions derived for all-cause mortality^{15,40} to estimate acute and chronic deaths given the global nature of this study. The estimated global acute and chronic deaths attributable to the 2023 Canadian wildfires varied by a factor of 4 (1,300–5,400) and

5 (31,000–152,000), respectively, when different exposure–response functions were used (Supplementary Tables 7 and 8; see Methods for details), indicating large variations in wildfire $\text{PM}_{2.5}$ exposure–response functions and the urgent need for well-designed epidemiological studies. Even still, the overall conclusion of this study, that is, the enormous

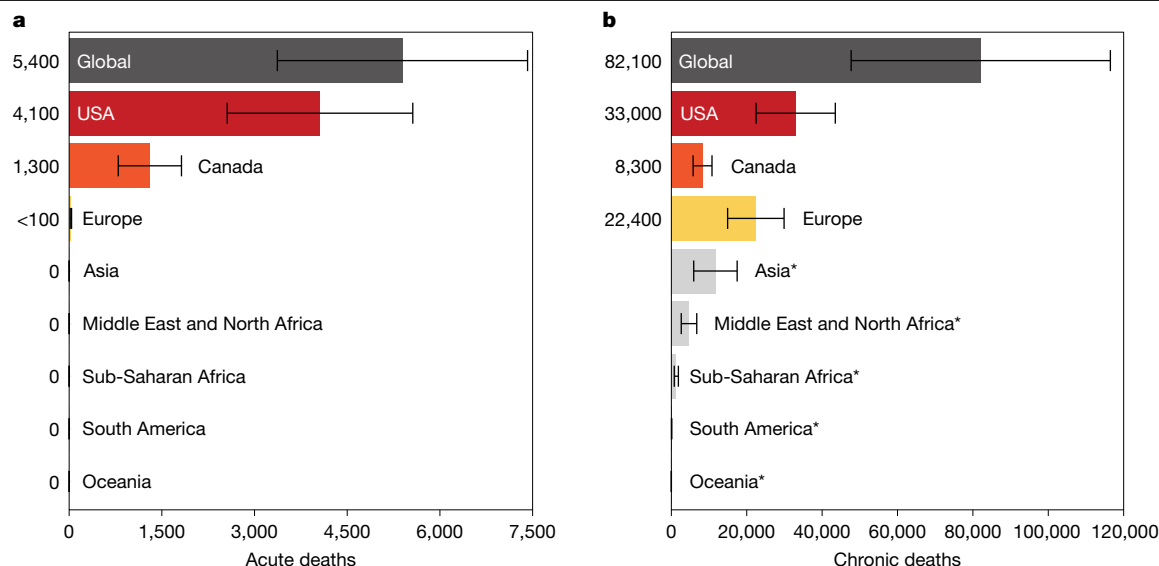


Fig. 4 | Global acute and chronic deaths attributable to the 2023 Canadian wildfires. a, Acute deaths. b, Chronic deaths. Errors bars denote the 95% CI of the estimates. The asterisk indicates regions where the Canadian-wildfire-related

annual mean $PM_{2.5}$ concentration is not statistically significant compared with the interannual variation of $PM_{2.5}$ concentration.

and far-reaching $PM_{2.5}$ pollution and health burden from a single large wildfire, remain robust.

Our findings are subject to several important uncertainties and limitations. Fire emissions have large uncertainties in general owing to errors in emission factors and estimates of fuel burned³⁷, which are then propagated within chemical transport models such as the GEOS-Chem model we use, leading to uncertainties in both simulated $PM_{2.5}$ concentrations and estimates of the contribution of fire emissions (Supplementary Figs. 15 and 16). Smoke-injection height is not considered in the GEOS-Chem simulation, which may lead to overestimates and underestimates of fire-related $PM_{2.5}$ concentration in the fire source region and the downwind region, respectively⁵¹. The all-source estimates of $PM_{2.5}$ exposure we develop are also subject to uncertainties derived from errors in input data and the machine-learning model itself (Supplementary Figs. 13 and 17). Finally, there are uncertainties in our estimates of attributable mortality owing to statistical methods and the limited epidemiology evidence on which exposure–response functions are based. In each case, we have assessed and quantified uncertainties by comprehensive analysis and sensitivity testing, integrating and aggregating errors in all steps through Monte Carlo, and we report 95% CIs for all of our main results. Further details about the calculation of uncertainties are in Methods.

Beyond these quantified uncertainties, we are cognizant of several limitations in our approach that might be improved by future studies. For example, the relatively coarse resolution of the GEOS-Chem model ($2^\circ \times 2.5^\circ$) may underestimate or overestimate fire-related pollution exposure^{52,53} (it is noted that the baseline exposures are resolved at $0.1^\circ \times 0.1^\circ$ resolution). Simulating long-range transport of wildfire-related $PM_{2.5}$ and quantifying its contribution to total $PM_{2.5}$ exposure are subject to uncertainties. After long-range transport, pollution from local sources may outweigh the contribution of the Canadian wildfires to the annual mean $PM_{2.5}$ concentration. The contribution of the 2023 Canadian wildfires was statistically significant over North America and Europe when compared with the interannual variability in $PM_{2.5}$ concentrations but statistically insignificant over other downwind regions (Methods and Supplementary Fig. 18).

The health impacts we estimate assume a uniform toxicity of different $PM_{2.5}$ species, which may underestimate the health impacts of wildfire emissions that have a higher proportion of carbonaceous aerosols whose toxicity tends to be greater than that of other species^{54,55}. Wildfire-related

$PM_{2.5}$ may also contain more oxidative and proinflammatory components that could increase oxidative potential during long-range transport, and thereby affect health effects in downwind regions^{56,57}. These factors are not accounted for in current $PM_{2.5}$ exposure–response functions and deserve further investigation. Although increased toxicity of wildfire-related $PM_{2.5}$ compared with all-source $PM_{2.5}$ has been observed, evidence of the health effects of wildfire-related $PM_{2.5}$ is still limited^{13,58–60}. In particular, some studies have reported mixed effects on acute health impacts in regions with limited sample size or varying analytic approaches^{15,59–61}. Our estimates of chronic mortality are also estimated using an exposure–response function for all-source $PM_{2.5}$ rather than for wildfire $PM_{2.5}$ given the lack of epidemiological evidence. Further well-designed epidemiological studies on this topic are urgently needed. In addition, we limit our analysis of fire-related health impacts to attributable mortality; numerous studies have reported non-fatal impacts of acute wildfire smoke exposure^{13,58}. Lastly, although we use ambient outdoor $PM_{2.5}$ concentrations as the indicator of $PM_{2.5}$ exposure during fire events, successfully limiting infiltration of $PM_{2.5}$ into indoor environments can substantially reduce such exposure and related health impacts. Further investigation of the changes in human behaviour and related $PM_{2.5}$ exposure during fire events will thus help to improve the accuracy of estimated health impacts in the future.

Nonetheless, our results robustly reveal that the 2023 Canadian wildfires led to substantial and extensive long-range $PM_{2.5}$ pollution and health impacts. Given recent trends in the frequency and severity of boreal and temperate wildfires⁶² and further projected increases in extreme fires under climate change^{33–35}, the global health impacts of the wildfires we assess can be expected to continue and grow in the future. Although many places are investing in efforts to manage wildfire risks via landscape-scale fuels management and early suppression, the vast extent and remoteness of many fire-prone forests presents a daunting and long-term task. In the meantime, accurate air-quality forecasting and pollution alert systems may be quick and cost-effective options for reducing human exposure to wildfire smoke^{63,64}. Given the relatively large differences among current fire emission inventories^{42,43}, such forecast and alert systems could benefit from improved fire emission estimates based on advanced satellite observations. Moreover, the transboundary wildfire impacts we demonstrate suggest the potential value of international cooperation to monitor and prevent extreme wildfires.

Online content

Any methods, additional references, Nature Portfolio reporting summaries, source data, extended data, supplementary information, acknowledgements, peer review information; details of author contributions and competing interests; and statements of data and code availability are available at <https://doi.org/10.1038/s41586-025-09482-1>.

- Canadian wildfire smoke puts around 70 million US residents under air quality alerts. *Cable News Network* <https://edition.cnn.com/2023/07/16/weather/canada-wildfires-us-air-quality-alerts-sunday/index.html> (2023).
- Wang, Z. et al. Severe global environmental issues caused by Canada's record-breaking wildfires in 2023. *Adv. Atmos. Sci.* **41**, 565–571 (2024).
- Schimel, D. & Baker, D. The wildfire factor. *Nature* **420**, 29–30 (2002).
- Friedlingstein, P. et al. Global Carbon Budget 2023. *Earth Syst. Sci. Data* **15**, 5301–5369 (2023).
- Bond, W. J., Woodward, F. I. & Midgley, G. F. The global distribution of ecosystems in a world without fire. *New Phytol.* **165**, 525–537 (2005).
- Kelly, L. T. et al. Fire and biodiversity in the Anthropocene. *Science* **370**, eabb0355 (2020).
- McClure, C. D. & Jaffe, D. A. US particulate matter air quality improves except in wildfire-prone areas. *Proc. Natl Acad. Sci. USA* **115**, 7901–7906 (2018).
- O'Dell, K., Ford, B., Fischer, E. V. & Pierce, J. R. Contribution of wildland-fire smoke to US PM_{2.5} and its influence on recent trends. *Environ. Sci. Technol.* **53**, 1797–1804 (2019).
- Burke, M. et al. The contribution of wildfire to PM_{2.5} trends in the USA. *Nature* **622**, 761–766 (2023).
- Xu, R. B. et al. Global population exposure to landscape fire air pollution from 2000 to 2019. *Nature* **621**, 521–529 (2023).
- Zhang, D. L. et al. Wildland fires worsened population exposure to PM_{2.5} pollution in the contiguous United States. *Environ. Sci. Technol.* **57**, 19990–19998 (2023).
- Johnston, F. H. et al. Estimated global mortality attributable to smoke from landscape fires. *Environ. Health Perspect.* **120**, 695–701 (2012).
- Reid, C. E. et al. Critical review of health impacts of wildfire smoke exposure. *Environ. Health Perspect.* **124**, 1334–1343 (2016).
- Cascio, W. E. Wildland fire smoke and human health. *Sci. Total Environ.* **624**, 586–595 (2018).
- Chen, G. B. et al. Mortality risk attributable to wildfire-related PM_{2.5} pollution: a global time series study in 749 locations. *Lancet Planet. Health* **5**, e579–e587 (2021).
- Canadian Interagency Forest Fire Centre. Wildfire graphs. *CIFFC* <https://ciffc.net/statistics> (2023).
- Byrne, B. et al. Carbon emissions from the 2023 Canadian wildfires. *Nature* **633**, 835–839 (2024).
- Meng, J. et al. Source contributions to ambient fine particulate matter for Canada. *Environ. Sci. Technol.* **53**, 10269–10278 (2019).
- Childs, M. L. et al. Daily local-level estimates of ambient wildfire smoke PM_{2.5} for the contiguous US. *Environ. Sci. Technol.* **56**, 13607–13621 (2022).
- Wei, J. et al. Long-term mortality burden trends attributed to black carbon and PM_{2.5} from wildfire emissions across the continental USA from 2000 to 2020: a deep learning modelling study. *Lancet Planet. Health* **7**, e963–e975 (2023).
- Wotawa, G. & Trainer, M. The influence of Canadian forest fires on pollutant concentrations in the United States. *Science* **288**, 324–328 (2000).
- Forster, C. et al. Transport of boreal forest fire emissions from Canada to Europe. *J. Geophys. Res. Atmos.* **106**, 22887–22906 (2001).
- Colarco, P. R. et al. Transport of smoke from Canadian forest fires to the surface near Washington, DC: injection height, entrainment, and optical properties. *J. Geophys. Res. Atmos.* **109**, D06203 (2004).
- DeBell, L. J. et al. A major regional air pollution event in the northeastern United States caused by extensive forest fires in Quebec, Canada. *J. Geophys. Res. Atmos.* **109**, D19305 (2004).
- Vaughan, G. et al. Transport of Canadian forest fire smoke over the UK as observed by lidar. *Atmos. Chem. Phys.* **18**, 11375–11388 (2018).
- Hung, W. T. et al. The impacts of transported wildfire smoke aerosols on surface air quality in New York State: a case study in summer 2018. *Atmos. Environ.* **227**, 117415 (2020).
- Yang, Z. F. et al. Influence of the transported Canadian wildfire smoke on the ozone and particle pollution over the mid-Atlantic United States. *Atmos. Environ.* **273**, 118940 (2022).
- McCracken, T., Chen, P., Metcalf, A. & Fan, C. Quantifying the impacts of Canadian wildfires on regional air pollution networks. *Sci. Total Environ.* **928**, 172461 (2024).
- Yu, M. Z., Zhang, S. Y., Ning, H., Li, Z. L. & Zhang, K. Assessing the 2023 Canadian wildfire smoke impact in northeastern US: air quality, exposure and environmental justice. *Sci. Total Environ.* **926**, 171853 (2024).
- Wen, J. F. et al. Quantifying fire-specific smoke exposure and health impacts. *Proc. Natl Acad. Sci. USA* **120**, e2309325120 (2023).
- Silver, B., Arnold, S. R., Reddington, C. L., Emmons, L. K. & Conibear, L. Large transboundary health impact of Arctic wildfire smoke. *Commun. Earth Environ.* **5**, 199 (2024).
- Stevens, R., Poterlot, C., Trieu, N., Rodriguez, H. A. & Hayes, P. L. Transboundary transport of air pollution in eastern Canada. *Environ. Sci. Adv.* **3**, 448–469 (2024).
- Xie, Y. Y. et al. Tripling of western US particulate pollution from wildfires in a warming climate. *Proc. Natl Acad. Sci. USA* **119**, e2111372119 (2022).
- Brown, P. T. et al. Climate warming increases extreme daily wildfire growth risk in California. *Nature* **621**, 760–766 (2023).
- Wang, S. S. C., Leung, L. R. & Qian, Y. Projection of future fire emissions over the contiguous US using explainable artificial intelligence and CMIP6 models. *J. Geophys. Res. Atmos.* **128**, e2023JD039154 (2023).
- Bey, I. et al. Global modeling of tropospheric chemistry with assimilated meteorology: model description and evaluation. *J. Geophys. Res. Atmos.* **106**, 23073–23095 (2001).
- Van Der Werf, G. R. et al. Global fire emissions estimates during 1997–2016. *Earth Syst. Sci. Data* **9**, 697–720 (2017).
- Koster, R. D., Darnenov, A. S. & da Silva, A. M. *The Quick Fire Emissions Dataset (QFED): Documentation of Versions 2.1, 2.2 and 2.4*. Report No. NASA/TM-2015-104606 (NASA, 2015).
- Kaiser, J. W. et al. Biomass burning emissions estimated with a global fire assimilation system based on observed fire radiative power. *Biogeosciences* **9**, 527–554 (2012).
- Chen, J. & Hoek, G. Long-term exposure to PM and all-cause and cause-specific mortality: a systematic review and meta-analysis. *Environ. Int.* **143**, 105974 (2020).
- Wei, J. et al. First close insight into global daily gapless 1 km PM_{2.5} pollution, variability, and health impact. *Nat. Commun.* **14**, 8349 (2023).
- Pan, X. H. et al. Six global biomass burning emission datasets: intercomparison and application in one global aerosol model. *Atmos. Chem. Phys.* **20**, 969–994 (2020).
- Carter, T. S. et al. How emissions uncertainty influences the distribution and radiative impacts of smoke from fires in North America. *Atmos. Chem. Phys.* **20**, 2073–2097 (2020).
- McDuffie, E. E. et al. Source sector and fuel contributions to ambient PM_{2.5} and attributable mortality across multiple spatial scales. *Nat. Commun.* **12**, 3594 (2021).
- Murray, C. J. L. et al. Global burden of 87 risk factors in 204 countries and territories, 1990–2019: a systematic analysis for the Global Burden of Disease Study 2019. *Lancet* **396**, 1223–1249 (2020).
- Xu, R. et al. Global, regional, and national mortality burden attributable to air pollution from landscape fires: a health impact assessment study. *Lancet* **404**, 2447–2459 (2024).
- Pope, I. I. et al. Mortality risk and fine particulate air pollution in a large, representative cohort of US adults. *Environ. Health Perspect.* **127**, 077007 (2019).
- Doubleday, A. et al. Mortality associated with wildfire smoke exposure in Washington state, 2006–2017: a case-crossover study. *Environ. Health* **19**, 4 (2020).
- Connolly, R. et al. Mortality attributable to PM_{2.5} from wildland fires in California from 2008 to 2018. *Sci. Adv.* **10**, ead11252 (2024).
- Orellano, P., Reynoso, J., Quaranta, N., Bardach, A. & Ciapponi, A. Short-term exposure to particulate matter (PM₁₀ and PM_{2.5}), nitrogen dioxide (NO₂), and ozone (O₃) and all-cause and cause-specific mortality: systematic review and meta-analysis. *Environ. Int.* **142**, 105876 (2020).
- Kahn, R. A. et al. Wildfire smoke injection heights: two perspectives from space. *Geophys. Res. Lett.* **35**, L04809 (2008).
- Fenech, S. et al. The influence of model spatial resolution on simulated ozone and fine particulate matter for Europe: implications for health impact assessments. *Atmos. Chem. Phys.* **18**, 5765–5784 (2018).
- Zhao, X. et al. Improving assessment of population exposure and health impacts to PM_{2.5} with high spatial and temporal data. *GISci. Remote Sens.* **61**, 2388921 (2024).
- Xu, R. B. et al. Wildfires, global climate change, and human health. *N. Engl. J. Med.* **383**, 2173–2181 (2020).
- Aguilera, R., Corringham, T., Gershunov, A. & Benmarhnia, T. Wildfire smoke impacts respiratory health more than fine particles from other sources: observational evidence from Southern California. *Nat. Commun.* **12**, 1493 (2021).
- Wong, J. P. S. et al. Effects of atmospheric processing on the oxidative potential of biomass burning organic aerosols. *Environ. Sci. Technol.* **53**, 6747–6756 (2019).
- Zhou, S., Xu, R. B., Chen, G. B., Yu, P. & Guo, Y. M. Where is the boundary of wildfire smoke? *Innov. Med.* **1**, 100024 (2023).
- Liu, J. C., Pereira, G., Uhl, S. A., Bravo, M. A. & Bell, M. L. A systematic review of the physical health impacts from non-occupational exposure to wildfire smoke. *Environ. Res.* **136**, 120–132 (2015).
- Grant, E. & Runkle, J. D. Long-term health effects of wildfire exposure: a scoping review. *J. Clim. Change Health* **6**, 100110 (2022).
- Gao, Y. et al. Long-term impacts of non-occupational wildfire exposure on human health: a systematic review. *Environ. Pollut.* **320**, 121041 (2023).
- Magzamen, S. et al. Differential cardiopulmonary health impacts of local and long-range transport of wildfire smoke. *GeoHealth* **5**, e2020GH000330 (2021).
- Senande-Rivera, M., Insua-Costa, D. & Miguez-Macho, G. Spatial and temporal expansion of global wildland fire activity in response to climate change. *Nat. Commun.* **13**, 1208 (2022).
- Pavlovic, R. et al. The FireWork air quality forecast system with near-real-time biomass burning emissions: recent developments and evaluation of performance for the 2015 North American wildfire season. *J. Air Waste Manage. Assoc.* **66**, 819–841 (2016).
- Kim, H. C., Chai, T. F., Stein, A. & Kondragunta, S. Inverse modeling of fire emissions constrained by smoke plume transport using HYSPLIT dispersion model and geostationary satellite observations. *Atmos. Chem. Phys.* **20**, 10259–10277 (2020).

Publisher's note Springer Nature remains neutral with regard to jurisdictional claims in published maps and institutional affiliations.



Open Access This article is licensed under a Creative Commons Attribution-NonCommercial-NoDerivatives 4.0 International License, which permits any non-commercial use, sharing, distribution and reproduction in any medium or format, as long as you give appropriate credit to the original author(s) and the source, provide a link to the Creative Commons licence, and indicate if you modified the licensed material. You do not have permission under this licence to share adapted material derived from this article or parts of it. The images or other third party material in this article are included in the article's Creative Commons licence, unless indicated otherwise in a credit line to the material. If material is not included in the article's Creative Commons licence and your intended use is not permitted by statutory regulation or exceeds the permitted use, you will need to obtain permission directly from the copyright holder. To view a copy of this licence, visit <http://creativecommons.org/licenses/by-nc-nd/4.0/>.

© The Author(s) 2025

Methods

Model framework

This study combines multiple datasets and models, as presented in Extended Data Fig. 1, to estimate the contribution of the 2023 Canadian wildfires to global $\text{PM}_{2.5}$ exposure and health impacts under a near-real-time framework (<http://tapdata.org.cn>). We also analyse two additional years, 2021 and 2017, which were reported as the years with the second- and third-largest wildfire emissions in Canada since 2000 (Extended Data Fig. 2b), for comparison. We first used the GEOS-Chem chemical transport model³⁶ at a spatial resolution of $2^\circ \times 2.5^\circ$ and 3 near-real-time global fire emission inventories, that is, the Global Fire Emissions Database version 4 with small fires (GFEDv4.1s)^{37,65}, the Quick Fire Emissions Dataset version 2.5 (QFEDv2.5r1)³⁸ and the Global Fire Assimilation System version 1.2 (GFASv1.2)³⁹, to simulate the global daily $\text{PM}_{2.5}$ concentrations and the fractional shares in total $\text{PM}_{2.5}$ concentrations contributed by wildfire emissions using a zero-out approach. Second, to improve the spatial resolution and accuracy of the global daily $\text{PM}_{2.5}$ estimation, we developed a machine-learning-based $\text{PM}_{2.5}$ retrieval model that combines data from multiple sources, including ground-monitoring measurements, satellite retrievals, reanalysis data and GEOS-Chem simulations, to estimate the global daily $\text{PM}_{2.5}$ concentrations at a spatial resolution of $0.1^\circ \times 0.1^\circ$. The $\text{PM}_{2.5}$ retrieval model was trained using GEOS-Chem simulations with the GFED, the QFED and the GFAS as a priori fire emissions, respectively, and three sets of global daily $\text{PM}_{2.5}$ estimates were derived. Then the retrieved total $\text{PM}_{2.5}$ concentrations based on the GFED, the QFED and the GFAS were multiplied by previously simulated fractional contributions with corresponding fire emissions, to obtain the $\text{PM}_{2.5}$ exposure attributable to wildfires. The performance of the three fire emission inventories in estimating fire-related $\text{PM}_{2.5}$ exposures was evaluated, and the GFED-based results were selected for presentation and further analysis to facilitate comparison with other recent studies that use similar approaches^{9–11,44}. To investigate the transboundary impact of Canadian wildfires globally and in North America, we further quantified the contributions of five regions' wildfires (that is, Eastern Canada, Western Canada, Eastern USA, Western USA and other global regions; Extended Data Fig. 3b) to $\text{PM}_{2.5}$ concentrations by conducting additional zero-out scenarios using the GFED emission inventory. Finally, we assessed the acute and chronic deaths attributable to $\text{PM}_{2.5}$ pollution from Canadian wildfires using previously established exposure–response functions^{15,40}. Further details of each analytical step are provided below.

Global fire emissions

A fire emission inventory is an essential input dataset for our analyses. We separately examined the impacts of fire emissions using three near-real-time fire emission inventories available for the year 2023, the GFED^{37,65}, the QFED³⁸ and the GFAS³⁹. The model results and fire-related $\text{PM}_{2.5}$ estimates using each of the three fire emissions datasets are discussed in 'Model evaluation'.

GFEDv4.1s. The GFED inventory was developed for use in large-scale modelling studies. The latest GFEDv4.1s used in this study is archived at <https://surfdrive.surf.nl/files/index.php/s/5y7TdE6ufwpkAW1>. It is based on 500-m Moderate Resolution Imaging Spectroradiometer (MODIS) burned area maps⁶⁶ supplemented with MODIS active fires converted to burned area⁶⁷. After 2016, emissions are derived from MODIS active fires scaled to emissions based on the 2001–2016 period when both datasets overlapped. Emission factors, mostly from ref. 68, are used to convert fire carbon emissions to trace gases and aerosols. The emissions, including carbon, dry matter, CO_2 , CO , NO_x , organic carbon, black carbon, $\text{PM}_{2.5}$, total particulate matter and SO_2 among others, are available from 1997 to 2023 at $0.25^\circ \times 0.25^\circ$ globally^{37,65}.

QFEDv2.5r1. The QFED inventory was developed by the National Aeronautics and Space Administration (NASA) and serves as the standard fire emissions in the GEOS data assimilation system and the Modern-Era Retrospective analysis for Research and Applications, version 2 (MERRA-2) reanalysis data products⁶⁹. In this study, QFEDv2.5r1 is used, which is available at <https://portal.nccs.nasa.gov/datashare/gmao/qfed/>. On the basis of a top-down approach, QFED obtains the fire radiative power (FRP) and location from satellite observations from MODIS Level 2 fire products and MODIS Geolocation products and calculates the open combustion of non-fossilized vegetative or organic fuel³⁸. It provides high spatiotemporal resolution and near-real-time global biomass burning emissions, including the $0.1^\circ \times 0.1^\circ$ daily emissions of black carbon, organic carbon, SO_2 , CO , CO_2 , $\text{PM}_{2.5}$, NH_3 , NO_x and so on, from 2001 to present.

GFASv1.2. The GFASv1.2 data are used for the Copernicus Atmosphere Monitoring Service (CAMS) global atmospheric composition and regional air-quality forecasts, which can be found at <https://ads.atmosphere.copernicus.eu/cdsapp#!/dataset/cams-global-fire-emissions-gfas?tab=overview/>. Fire emissions are calculated based on FRP measurements from two MODIS instruments onboard NASA's Terra and Aqua satellite that are first converted to estimates of the dry matter consumed by fire and then to emissions using biome-specific emission factors. The GFAS provides daily averaged biomass burning and vegetation fire emissions for 40 pyrogenic species (aerosols, reactive gases and greenhouse gases) from 2003 to the present, with a spatial resolution of $0.1^\circ \times 0.1^\circ$ (ref. 39).

GEOS-Chem simulation

Using each of the three fire emission inventories (that is, the GFED, the QFED and the GFAS), we estimated the global $\text{PM}_{2.5}$ concentrations using the three-dimensional global chemical transport model GEOS-Chem³⁶. These concentrations are an important input to our $\text{PM}_{2.5}$ retrieval model ('Retrieval of global $\text{PM}_{2.5}$ based on multi-source data fusion') and are used to quantify the fractional contributions of wildfire emissions to total $\text{PM}_{2.5}$ concentrations ('Estimation of fire-specific $\text{PM}_{2.5}$ exposure' and 'Fire source attribution'). GEOS-Chem has been used by numerous previous studies to simulate smoke pollution from wildfires^{8,43,70–76}.

GEOS-Chem v.14.0.1 (<https://zenodo.org/records/7271974/>) is used in this study. The near-real-time meteorological data from the Goddard Earth Observation System-Forward Processing (GEOS-FP)⁷⁷ of the NASA Global Modeling and Assimilation Office (GMAO) was used to drive the GEOS-Chem model. The GEOS-FP data span the time period from 2011 to the present, with a native resolution of $0.25^\circ \times 0.3125^\circ$ and 72 vertical levels. We reduce the vertical levels to 47 and the spatial resolution to $2.0^\circ \times 2.5^\circ$ to support the global chemical transport simulations. GEOS-Chem uses standard full chemistry with detailed oxidant–aerosol chemistry. Sulfate–nitrate–ammonium aerosol thermodynamics are computed with ISORROPIA v2.2⁷⁸.

All emissions in GEOS-Chem are configured by HEMCO (Harmonized Emissions Component) 3.0⁷⁹, to combine and regrid the different emissions. The global anthropogenic emissions (including shipping) of NO_x , SO_2 , CO , NH_3 , black carbon, organic carbon and volatile organic compounds are provided by the Community Emissions Data System (CEDS) v2 inventory (<https://data.pnnl.gov/dataset/CEDS-4-21-21/>)⁸⁰. Aircraft emissions are from the Aviation Emissions Inventory Code (AEIC)⁸¹ inventory. For global fire emissions, GFEDv4.1s, QFEDv2.5r1 and GFASv1.2 are used respectively. Dust⁸², sea salt⁸³, lighting NO_x (ref. 84), soil NO_x (ref. 85) and biogenic volatile organic compounds (MEGAN v2.1⁸⁶) are calculated online in HEMCO. We use the non-local scheme implemented in ref. 87 for the boundary-layer mixing in GEOS-Chem, which emits all emissions into the atmospheric boundary layer, including wildfire emissions.

Retrieval of global $\text{PM}_{2.5}$ based on multi-source data fusion

We estimate the global daily $\text{PM}_{2.5}$ exposures from all sources at a $0.1^\circ \times 0.1^\circ$ horizon resolution using a multilayer machine-learning

retrieval model that fuses data from ground-monitoring measurements, satellite retrievals, GEOS-Chem model simulations, meteorological fields, reanalysis data and population distribution. The structure of the PM_{2.5} retrieval model is illustrated in Supplementary Fig. 1. We separately train our retrieval model with GEOS-Chem simulations based on the GFED, the QFED and the GFAS emissions (but with the same model structure) to derive three sets of global PM_{2.5} concentration estimates. Further details about the data sources and the model structure are provided below.

Ground measurements. We collected PM_{2.5} surface monitoring data from different global regions as model input. We obtained surface PM_{2.5} measurements in Canada from Environmental Canada (<https://data-donnees.az.ec.gc.ca/data/air/monitor/national-air-pollution-surveillance-naps-program/Data-Donnees/>). We obtained PM_{2.5} measurements in the USA from the US Environmental Protection Agency (US EPA) AirNow (<https://www.epa.gov/outdoor-air-quality-data/download-daily-data>) and from the Interagency Monitoring of Protected Visual Environments (IMPROVE) (<https://views.cira.colostate.edu/fed/QueryWizard/Default.aspx>). To improve the representation of air pollution, we also collected PM_{2.5} monitoring data from: the AirFire programme of the US Forest Service (<https://info.airfire.org/airmonitor-package>) for the USA; the European Air Quality Portal (<https://eadmz1-cws-wp-air02.azurewebsites.net/>) for Europe; the China National Environmental Monitoring Center (CNEMC; <http://www.cnemc.cn/>) for China; and the OpenAQ (<https://openaq.org/>) for other regions around the world. Hourly measurements were averaged as daily records and only daily records generated from at least 16 hourly data points were included. In summary, we collected approximately 453,000 valid daily records from about 1,610 monitors in North America, approximately 567,000 valid daily records from about 2,010 stations in Europe, approximately 612,000 valid daily records from about 1,720 stations in China, as well as approximately 68,000 valid daily records from about 850 stations in other regions for the year 2023.

Aerosol optical depth. Satellite aerosol optical depth (AOD) retrievals were extracted from the MODIS Level 2 aerosol products (MOD04 and MYD04) at a 0.1° spatial resolution⁸⁸. To improve the data coverage and better reflect the aerosol loading during the day, we first fused the AOD retrievals from the Dark Target algorithm and the Deep Blue algorithm with daily linear regressions, and then fused the AOD from the Aqua and Terra satellites with daily linear regressions. As considerable gaps in the AOD data still existed after this data fusion, we used the CAMS modelling and reanalysis data (<https://ads.atmosphere.copernicus.eu>)⁸⁹ with complete coverage to provide information on the spatial distribution of aerosols. CAMS parameters, including the AOD at 550 nm, black carbon AOD, organic carbon AOD, wildfire combustion rate, FRP and total column carbon monoxide, were adopted in the model. The MODIS AOD and various CAMS AODs were treated as separate predictors in the retrieval model.

GEOS-Chem simulations. The PM_{2.5} simulations from GEOS-Chem were used in this model. As three fire emission inventories were used in GEOS-Chem to simulate surface PM_{2.5} concentrations, we constructed three model training datasets with different GEOS-Chem simulations using the GFED, the QFED and the GFAS, respectively.

Other ancillary data. Smoke plume information in North America was collected from the Hazard Mapping System (HMS; <https://www.ospo.noaa.gov/Products/land/hms.html#about>)⁹⁰, provided by the National Oceanic and Atmospheric Administration/National Environmental Satellite, Data, and Information Service (NOAA/NESDIS). The density-assigned and time-marked plumes polygons were manually generated from GOES-16 and GOES-17 ABI true-colour imagery. We assigned the time-specific plume data to daily plume density and included it in the model to provide valuable information on smoke plume distributions in North America. Meteorological fields, including daily average air temperature at 2 m, specific humidity at 2 m, relative

humidity, surface pressure, boundary-layer height, total latent energy flux, evaporation from turbulence, *U* and *V* wind components at 10 m, and total precipitation, were extracted from GEOS-FP reanalysis data at a spatial resolution of 0.25° × 0.3125° and downscaled to the 0.1° modelling grid by the inverse distance weighting algorithm. The gridded population distribution data for 2020 were obtained from WorldPop (<https://www.worldpop.org/>) at a resolution of 30 arcseconds^{91,92} and we assumed a constant population distribution in 2017, 2021 and 2023. We constrained the gridded WorldPop population data with national total population for each year from the United Nations (<https://population.un.org/wpp/>)⁹³, US Census Bureau, Population Division (<https://www.census.gov/data/tables/time-series/demo/popest/2020s-state-total.html>)⁹⁴ and Statistics Canada (<https://www150.statcan.gc.ca/>)¹⁶.

Model structure. The total PM_{2.5} retrieval model was designed with a three-layer random forest structure following our previous work⁹⁵ (Supplementary Fig. 1). The first-layer model predicts the high-pollution index, which is a binary variable indicating whether the station-day concentration is higher than the mean plus two standard deviations of PM_{2.5} concentrations of the corresponding station and month. In our previous work⁹⁶, we found that a two-layer model including the high-pollution indicator and the Synthetic Minority Over-sampling Technique (SMOTE) resampling algorithm can correct the low-bias from the unbalanced training sample of high-pollution events. Following the approach, we applied the SMOTE resampling algorithm to increase the representation of high-pollution events in the model training samples. The second-layer model uses the prediction of high-pollution index as a predictor to predict the total PM_{2.5} concentrations. Previous studies have shown that the model trained with the residual can correct the systematic bias and improve the model prediction accuracy^{97,98}. The third-layer model then predicts the residual between PM_{2.5} predictions and measurements and was trained by with-fire samples and no-fire samples separately, to highlight the potential differences in PM_{2.5} characteristics during fire events. Here the with-fire samples were defined as samples with CAMS combustion rate > 0 or the HMS plume density > 0 (refs. 8, 9). The final PM_{2.5} concentration estimation is the prediction from the second-layer model plus the prediction from the third-layer model. The model was trained separately with data for 2023, 2021 and 2017 as well as with GEOS-Chem simulations with the GFED, the QFED and the GFAS emissions.

Estimation of fire-specific PM_{2.5} exposure

PM_{2.5} exposure attributable to wildfire emissions was then estimated using three fire emissions, respectively. In detail, the wildfire-related PM_{2.5} was quantified by multiplying the GEOS-Chem simulated fire contributions to total PM_{2.5} by the retrieved all-source PM_{2.5} concentrations. Supplementary Table 1 summarizes the GEOS-Chem simulations used in this study. We conducted the GEOS-Chem simulations with the GFED, the QFED and the GFAS inventories separately (that is, 'base' in Supplementary Table 1) as well as the no-fire GEOS-Chem simulation that turned off global fire emissions (that is, 'nofire' in Supplementary Table 1). All other emissions mentioned in 'GEOS-Chem simulation' are the same in the base and nofire simulations. Then the fraction of PM_{2.5} concentrations attributable to wildfires was calculated by equation (1) on a 2° × 2.5° grid, as determined by the GEOS-Chem model. We constructed three sets of wildfire-fraction data from the GEOS-Chem simulations driven by the three fire emissions. Likewise, the anthropogenic-related PM_{2.5} was calculated using equation (2) with similar model runs (turning off anthropogenic emissions, that is, 'noanthro' in Supplementary Table 1). The contributions from sources other than wildfires and anthropogenic activities were then obtained by subtracting their contributions from the total as in equation (3):

$$F_{\text{fire},k} = \text{GC}_{\text{fire},k} / \text{GC}_{\text{base},k} = (\text{GC}_{\text{base},k} - \text{GC}_{\text{nofire}}) / \text{GC}_{\text{base},k} \quad (1)$$

$$F_{\text{anthro},k} = \text{GC}_{\text{anthro},k} / \text{GC}_{\text{base},k} = (\text{GC}_{\text{base},k} - \text{GC}_{\text{noanthro},k}) / \text{GC}_{\text{base},k} \quad (2)$$

$$F_{\text{other},k} = 1 - F_{\text{fire},k} - F_{\text{anthro},k} \quad (3)$$

where the subscript k represents the three fire emissions, that is, GFED, QFED and GFAS. $\text{GC}_{\text{base},k}$ and $\text{GC}_{\text{noanthro},k}$ represent the GEOS-Chem-simulated $\text{PM}_{2.5}$ concentrations from the base and noanthro scenarios using fire emissions k , respectively. $\text{GC}_{\text{nofire}}$ represents the simulation with fire emissions turned off. $F_{\text{fire},k}$, $F_{\text{anthro},k}$ and $F_{\text{other},k}$ represent the fractional contribution of wildfires, anthropogenic and other emissions to $\text{PM}_{2.5}$ estimated from fire emissions k , respectively.

Then we spatially match the $\text{PM}_{2.5}$ fractions from GEOS-Chem simulations ($2^\circ \times 2.5^\circ$) with the $0.1^\circ \text{PM}_{2.5}$ retrievals through bilinear interpolation. The $\text{PM}_{2.5}$ retrievals were multiplied by the corresponding fractions to get the fire-related, anthropogenic-related and other-source-related $\text{PM}_{2.5}$, as shown in equations (4)–(6):

$$C_{\text{fire},k} = C_{\text{PM},k} \times F_{\text{fire},k} = C_{\text{PM},k} \times (\text{GC}_{\text{fire},k} / \text{GC}_{\text{base},k}) \quad (4)$$

$$C_{\text{anthro},k} = C_{\text{PM},k} \times F_{\text{anthro},k} = C_{\text{PM},k} \times (\text{GC}_{\text{anthro},k} / \text{GC}_{\text{base},k}) \quad (5)$$

$$C_{\text{other},k} = C_{\text{PM},k} \times F_{\text{other},k} \quad (6)$$

where $C_{\text{PM},k}$ represents the total $\text{PM}_{2.5}$ concentrations estimated from the machine-learning-based model using fire emissions k ($k = \text{GFED}$, QFED , GFAS) in ‘Retrieval of global $\text{PM}_{2.5}$ based on multi-source data fusion’, $C_{\text{fire},k}$, $C_{\text{anthro},k}$ and $C_{\text{other},k}$ represent the fire-, anthropogenic- and other-source-related $\text{PM}_{2.5}$ concentrations based on fire emissions k .

Model evaluation

Our models were fully evaluated at each step of the construction of fire-related $\text{PM}_{2.5}$ concentrations (Extended Data Fig. 1): the performance of the GEOS-Chem $\text{PM}_{2.5}$ simulations, the performance of the $\text{PM}_{2.5}$ retrieval model and the performance of $\text{PM}_{2.5}$ retrievals during fire events. Models based on the three fire emissions (GFED, QFED and GFAS) were compared in all the evaluations to understand the impacts of fire emissions on model performance. Total and fire-related $\text{PM}_{2.5}$ concentrations estimated using the three fire emissions were compared with each other. We also quantified the wildfire-related $\text{PM}_{2.5}$ estimates in previous years (2017 and 2021) and compared them with other studies as an additional evaluation of our methods.

Evaluation of GEOS-Chem $\text{PM}_{2.5}$ simulations. The annual average GEOS-Chem $\text{PM}_{2.5}$ concentrations driven by three fire emission inventories (GFED, QFED and GFAS) were evaluated against $\text{PM}_{2.5}$ ground observations in Canada and the USA (Supplementary Fig. 15). In Canada, the modelled $\text{PM}_{2.5}$ correlated reasonably well with ground observations, with R ranging between 0.41 and 0.69 and normalized model bias (NMB) between 0.01 and 0.72 for the three fire emissions. We noticed one outlier with unrealistically high $\text{PM}_{2.5}$ simulations in Canada resulted from high fire emission estimates; therefore, we also reported evaluation statistics without this data point to avoid the effects of an outlier (Supplementary Fig. 15). After removing the outlier, R between modelled and observed $\text{PM}_{2.5}$ increased from 0.41–0.69 to 0.66–0.82 and NMB was reduced from 0.01–0.72 to –0.04–0.30 in Canada. In the USA, simulations based on the three fire emissions had comparable performance against ground observations, with R between 0.46 and 0.47. As the only differences in these simulations are the underlying fire emission inventories, the differences in model performance can be solely attributed to the inventories. Compared with the GEOS-Chem simulation with the GFED inventory, using the QFED inventory helps to

reduce both the overestimates of $\text{PM}_{2.5}$ concentration in Canada (NMB from 0.30 to 0.16) and the underestimates in the USA (NMB from –0.22 to –0.06), whereas using the GFAS inventory reduces the overestimates of $\text{PM}_{2.5}$ concentration in Canada (NMB from 0.30 to –0.04) but gives similar results to GFED in the USA (NMB from –0.22 to –0.27). By comparing estimates of fire-related $\text{PM}_{2.5}$ exposure from different fire emission inventories in this way, we can evaluate the effects of GEOS-Chem model performance on the results (‘Comparisons of fire-related $\text{PM}_{2.5}$ among three fire emissions and with previous studies’).

Evaluation of $\text{PM}_{2.5}$ retrieval model. The $\text{PM}_{2.5}$ retrieval model was evaluated by both station-based and sample-based 20-fold cross-validation. The model training dataset was randomly divided into 20 equal folds according to air-quality monitoring stations and station-day observations, separately. Then the model was trained on 19 of these folds and tested on the remaining fold. This process was repeated 20 times until each fold of the data was used for testing once. The model performance was quantified by the comparisons between cross-validation predictions and ground measurements at the daily, monthly and yearly levels to reflect model uncertainties at different temporal scales (Extended Data Fig. 8 and Supplementary Fig. 13). In addition, to highlight the model’s ability in retrieving daily variations in $\text{PM}_{2.5}$ when controlling the seasonal and spatial variations, we included month-intercept (fix-month R^2) as well as month and station intercepts (fix-month-and-station R^2) when computing R^2 (within R^2) of the 20-fold cross-validation predictions following a previous study¹⁰ (Supplementary Table 5). We also calculated the station-specific R^2 to show the variations in model performance in space. Evaluation results of the retrieval models trained with GEOS-Chem simulations using the three fire emissions in 2023 are listed in Extended Data Fig. 8, Supplementary Fig. 13 and Supplementary Table 5. As the HMS data are available for only North America, we assessed the impact of including HMS data on global $\text{PM}_{2.5}$ retrievals. As shown in Supplementary Fig. 17, inclusion of the HMS data in the model led to substantial differences in $\text{PM}_{2.5}$ retrievals over North America whereas it had minor impacts in other regions. Therefore, we incorporated the HMS data as a predictor to improve the accuracy of wildfire-related $\text{PM}_{2.5}$ estimates in North America.

Globally, the retrieval model characterizes variations in $\text{PM}_{2.5}$ well, and models based on the GFED, the QFED and the GFAS performed similarly well under both the station-based and sample-based 20-fold cross-validation. The station-based 20-fold cross-validation R^2 ranged between 0.84 and 0.85 (RMSE between $8.55 \mu\text{g m}^{-3}$ and $8.62 \mu\text{g m}^{-3}$) at the daily scale, all equal to 0.88 (RMSE between $5.80 \mu\text{g m}^{-3}$ and $5.95 \mu\text{g m}^{-3}$) at the monthly scale, and ranged between 0.87 and 0.88 (RMSE between $4.80 \mu\text{g m}^{-3}$ and $5.00 \mu\text{g m}^{-3}$), in the year 2023. The sample-based cross-validation results are comparable to the station-based cross-validation results, indicating robust model performance in regions with limited observations. All models trained with the three fire emission inventories showed only a slight decrease in R^2 when controlling the seasonal and spatial variations (that is, fix-month R^2 between 0.86 and 0.88, and fix-month-and-station R^2 between 0.80 and 0.82), indicating the model’s ability to capture daily variations in $\text{PM}_{2.5}$ (Supplementary Table 5). Spatially, the global median station-specific R^2 was 0.79, 0.79 and 0.79 with 90% of station-specific R^2 above 0.37, 0.36 and 0.37 for models based on the GFED, the QFED and the GFAS, respectively. Our model performances are comparable to previous studies developing a global $\text{PM}_{2.5}$ retrieval model, in that the cross-validation R^2 of daily retrievals is around 0.91 and the RMSE ranges between $8.4 \mu\text{g m}^{-3}$ and $9.2 \mu\text{g m}^{-3}$ (refs. 10, 41).

Regionally we found a lower R^2 in Canada, which is mainly caused by several outliers in Canada resulting from unrealistically high GEOS-Chem simulations mentioned in ‘Evaluation of GEOS-Chem $\text{PM}_{2.5}$ simulations’. To avoid the influence of these occasional outliers on model evaluation, we reported the model performance after

removing data points outside 2σ of the Cook's distance of linear regression (Supplementary Table 5). Models based on the three fire emissions performed comparably well after removing the outliers. As these outliers of the retrieved $\text{PM}_{2.5}$ concentration occurred in a few days and in remote regions with sparse population, they do not considerably affect our exposure assessment and health burden quantification.

Evaluation of $\text{PM}_{2.5}$ retrievals during fire events. To assess the model's performance in capturing fire-related $\text{PM}_{2.5}$ variations, we further evaluated the model performance during fire events (Extended Data Fig. 9 and Supplementary Table 4)—when the $\text{PM}_{2.5}$ is dominated by wildfires. We first identified several major fire events and then compared the station-day observations during these fire events with the sample-based 20-fold cross-validation predictions. Thus, the station-day observations selected for evaluations were excluded from the model training to reveal the model performance in regions and periods without observations. We identified fire events with a similar protocol reported by an earlier work¹⁰, mainly according to the variations in $\text{PM}_{2.5}$ observations. A station-day is labelled as affected by wildfires when (1) it is during one of the manually identified fire events that showed a substantial increase in national daily average $\text{PM}_{2.5}$ monitoring time series data in Canada and the USA, separately. (2) The daily average $\text{PM}_{2.5}$ concentration is higher than the median of all the station-day records during this fire event. Here we used the median as cut-off number rather than selecting one station with the largest increase because one station's data were not sufficient to support the validation. (3) The $\text{PM}_{2.5}$ concentration is higher than twice the background $\text{PM}_{2.5}$ concentration before the fire season (first 2 months in 2023) at the corresponding station. (4) The $\text{PM}_{2.5}$ concentration is higher than $15 \mu\text{g m}^{-3}$, the WHO air-quality guidelines level. In total, 11 and 9 fire events were identified in Canada and the USA, respectively. The events lasted between 3 days and 23 days. The national fire-related $\text{PM}_{2.5}$ exposure during these fire events accounted for 83% and 81% of the annual fire-related $\text{PM}_{2.5}$ exposure in Canada and the USA, respectively, indicating that most significant fire events were identified by this method.

In North America, the three retrieval models with different fire emissions correctly reflected $\text{PM}_{2.5}$ variations during the fire events, with similar cross-validation R^2 ranging between 0.78 and 0.80 in the USA, but moderately different R^2 between 0.59 and 0.75 in Canada (Supplementary Table 4). We also noticed that as previously reported^{41,99}, our model still slightly underestimated $\text{PM}_{2.5}$ levels during extreme fire events with NMB ranging between -0.14 and -0.09 and between -0.13 and -0.10 for Canada and the USA, respectively.

Comparisons of fire-related $\text{PM}_{2.5}$ among the three fire emissions and with previous studies. To further understand the impacts of different fire emissions on total and fire-related $\text{PM}_{2.5}$ estimates, we compared the spatial and temporal distributions of our results among the three fire emissions (Supplementary Table 6). The spatial correlation was calculated using 3-year averaged gridded $\text{PM}_{2.5}$ data among models based on the 3 fire emissions, whereas the temporal correlation was calculated using daily population-weighted mean $\text{PM}_{2.5}$ concentrations for 3 years among models based on the 3 fire emissions. Some previous studies^{9–11,44} have investigated the impact of wildfires on $\text{PM}_{2.5}$ exposure other than the 2023 Canadian extreme wildfires. We also compared our fire-related $\text{PM}_{2.5}$ estimates with those previous studies as additional evaluations.

For spatial comparisons, the all-source $\text{PM}_{2.5}$ estimates based on the three fire emission inventories showed similar spatial distributions to high correlations globally (all pairwise Pearson correlation coefficients r were 0.99). The spatial distributions of fire-related $\text{PM}_{2.5}$ were also highly correlated between different emissions at the global scale, with pairwise r ranging between 0.88 and 0.95. The spatial patterns between the QFED-based and the GFAS-based estimates were more similar in specific regions than the GFED-base results, as fire emissions from

the QFED and the GFAS were estimated using a similar approach based on FRP from the MODIS instrument. For temporal comparisons, the population-weighted daily mean all-source $\text{PM}_{2.5}$ estimates showed high correlations at both the global scale (all pairwise Pearson correlation coefficients r were 0.99) and the regional scale. The fire-related $\text{PM}_{2.5}$ estimates had some temporal differences globally among the 3 inventories, but showed even higher correlations in Canada and the USA, with pairwise r of fire-related $\text{PM}_{2.5}$ ranging between 0.94 and 0.99 in Canada and between 0.94 and 0.97 in the USA.

Supplementary Fig. 14 shows the comparisons of estimated population-weighted fire-related $\text{PM}_{2.5}$ in Canada and the USA based on the three inventories, as well as their comparisons with previous studies^{9–11,44}. The fire-related $\text{PM}_{2.5}$ in Canada and the USA based on the three inventories showed consistent increasing trends in 2017, 2021 and 2023; however, the magnitudes of the estimated fire-related $\text{PM}_{2.5}$ varied between inventories, with the GFAS showing the lowest and the QFED showing the highest. In Canada, fire-related annual $\text{PM}_{2.5}$ exposure estimated with the 3 inventories showed good agreement ($3.75\text{--}4.49 \mu\text{g m}^{-3}$, relative difference within 20%). Given their similar fire-related $\text{PM}_{2.5}$ exposure estimates in Canada, the choice of fire inventory has a relatively minor effect on our overall conclusions. In the USA, the GFED-based and the GFAS-based estimates on fire-related annual $\text{PM}_{2.5}$ exposure in 2023 are also similar ($1.96 \mu\text{g m}^{-3}$ and $1.83 \mu\text{g m}^{-3}$, respectively), whereas the QFED-based estimates ($3.11 \mu\text{g m}^{-3}$) are 59–70% higher, consistent with several other recent studies (Supplementary Fig. 14). Because the GEOS-Chem $\text{PM}_{2.5}$ simulations with the QFED inventory show better agreement with surface observations in the USA, our estimates of fire-related contributions to $\text{PM}_{2.5}$ may be underestimated in the USA when using the GFED inventory.

Our population-weighted estimates of fire-related $\text{PM}_{2.5}$ based on GFED emissions in 2017 ($1.62 \mu\text{g m}^{-3}$ in Canada and $1.16 \mu\text{g m}^{-3}$ in the USA) are nearly identical to estimates by a previous study that used GFED emissions from 2000–2019¹⁰ ($1.50 \mu\text{g m}^{-3}$ in Canada and $1.21 \mu\text{g m}^{-3}$ in the USA). Another study⁴⁴ estimated the source contribution to ambient $\text{PM}_{2.5}$ in 2017 globally using GFED fire emissions and reported that the population-weighted fire-related $\text{PM}_{2.5}$ in Canada and the USA was $1.35 \mu\text{g m}^{-3}$ and $0.90 \mu\text{g m}^{-3}$, respectively, again similar to the GFED-based and the GFAS-based estimates. In addition, ref. 11 developed a data fusion model to divide the fire-source and other-source $\text{PM}_{2.5}$ in the USA and estimated that the mean fire-source $\text{PM}_{2.5}$ concentrations inside and outside the vicinity of an EPA air-quality monitoring station (defined by a 5-km radius) in 2017 are $0.97 \mu\text{g m}^{-3}$ and $0.92 \mu\text{g m}^{-3}$, respectively, also close to our GFED-based and GFAS-based estimates.

In summary, although the GFED, the QFED and the GFAS inventories show varied air-pollutant emissions and led to different fire-related $\text{PM}_{2.5}$ concentrations in GEOS-Chem simulations, the total $\text{PM}_{2.5}$ retrieval models with different fire emission inventories showed generally consistent performance. For the fire-related $\text{PM}_{2.5}$ concentrations, the GFED-based and the GFAS-based estimates are similar and more comparable to previous studies^{9–11,44}. We understand that each fire inventory has its own advantages and disadvantages; therefore, we cannot justify which one is the best. Given that the GFED has frequently been used in recent analyses^{8,10,12,43}, to put our results in the context with the literature, we choose to present the GFED-based estimates in the main text.

Fire source attribution

To further quantify the contributions of fires from different regions in North America, we divided Canada and the USA into four regions, Eastern Canada (CE), Western Canada (CW), Eastern USA (UE) and Western USA (UW) (Extended Data Fig. 3b). According to the EPA's delineation of North American ecological regions (Supplementary Fig. 2; <https://www.epa.gov/eco-research/ecoregions-north-america/>), the Level I ecoregions divide North America into 15 broads. It can be seen that the majority of Canada is covered by forests, whereas the eastern and

western parts of the USA are separated by plains and deserts. Therefore, we defined the above four regions according to administrative divisions in combination with the ecological regions in this study.

We then implemented simulations with regional wildfire emissions turned off using the GFED emissions (Supplementary Table 2). In addition, given that the zero-out approach may lead to additional bias owing to the nonlinear relationship between emissions and modelled $PM_{2.5}$ concentrations, the case of 'offNA' is used to evaluate this impact and constrain the results. The regional contributions can be calculated using equations (7)–(11):

$$\begin{aligned} \text{Scale} = & (GC_{\text{base,GFED}} - GC_{\text{offNA,GFED}}) \\ & / [(GC_{\text{base,GFED}} - GC_{\text{offCE,GFED}}) \\ & + (GC_{\text{base,GFED}} - GC_{\text{offCW,GFED}}) \\ & + (GC_{\text{base,GFED}} - GC_{\text{offUE,GFED}}) \\ & + (GC_{\text{base,GFED}} - GC_{\text{offUW,GFED}})] \end{aligned} \quad (7)$$

$$F_{\text{fireCE,GFED}} = \text{Scale} \times (GC_{\text{base,GFED}} - GC_{\text{offCE,GFED}}) / GC_{\text{base,GFED}} \quad (8)$$

$$F_{\text{fireCW,GFED}} = \text{Scale} \times (GC_{\text{base,GFED}} - GC_{\text{offCW,GFED}}) / GC_{\text{base,GFED}} \quad (9)$$

$$F_{\text{fireUE,GFED}} = \text{Scale} \times (GC_{\text{base,GFED}} - GC_{\text{offUE,GFED}}) / GC_{\text{base,GFED}} \quad (10)$$

$$F_{\text{fireUW,GFED}} = \text{Scale} \times (GC_{\text{base,GFED}} - GC_{\text{offUW,GFED}}) / GC_{\text{base,GFED}} \quad (11)$$

where $GC_{\text{offCE,GFED}}$, $GC_{\text{offCW,GFED}}$, $GC_{\text{offUE,GFED}}$, $GC_{\text{offUW,GFED}}$ and $GC_{\text{offNA,GFED}}$ are the GEOS-Chem-simulated $PM_{2.5}$ concentrations using the GFED emissions under the offCE, offCW, offUE, offUW and offNA scenarios, respectively. $F_{\text{fireCE,GFED}}$, $F_{\text{fireCW,GFED}}$, $F_{\text{fireUE,GFED}}$ and $F_{\text{fireUW,GFED}}$ are the fractional contributions to the $PM_{2.5}$ concentrations from fire emissions in CE, CW, UE and UW, respectively.

The zero-out approach used here may introduce additional bias due to the nonlinear relationship between emissions and modelled $PM_{2.5}$ concentrations. The bias can be calculated as equation (12):

$$\begin{aligned} \text{Bias} = & (GC_{\text{base,GFED}} - GC_{\text{offNA,GFED}}) \\ & - [(GC_{\text{base,GFED}} - GC_{\text{offCE,GFED}}) \\ & + (GC_{\text{base,GFED}} - GC_{\text{offCW,GFED}}) \\ & + (GC_{\text{base,GFED}} - GC_{\text{offUE,GFED}}) \\ & + (GC_{\text{base,GFED}} - GC_{\text{offUW,GFED}})] \end{aligned} \quad (12)$$

The absolute and relative biases due to nonlinearity are presented in Supplementary Fig. 16. Over the four regions, the absolute biases range from $-0.009 \mu\text{g m}^{-3}$ to $0.012 \mu\text{g m}^{-3}$, and the relative biases range from -1.35% to -0.09% , indicating that the biases related to nonlinear effects are relatively small.

To investigate the significance of the Canadian wildfire impact on the interannual variability in $PM_{2.5}$ concentrations in downwind regions, we compared the estimated annual mean $PM_{2.5}$ concentrations from the 2023 Canadian wildfires with 2000–2023 satellite-derived annual $PM_{2.5}$ concentrations (<https://sites.wustl.edu/acag/datasets/surface-pm2-5/#V6.GL.02.03/>)¹⁰⁰ and 2014–2023 annual mean $PM_{2.5}$ observations over the USA and Europe (Supplementary Fig. 18). When comparing with the interannual variability in $PM_{2.5}$ concentrations, the contribution of the 2023 Canadian wildfires was statistically significant in North America and Europe whereas it was statistically insignificant over other downwind regions. In the USA, the 2023 Canadian wildfires contributed to an average of $1.50 \mu\text{g m}^{-3}$ annual mean $PM_{2.5}$ over the locations of the EPA sites, larger than the differences in observed the $PM_{2.5}$ concentration between 2022 and 2023 ($0.99 \mu\text{g m}^{-3}$) as well as

the mean interannual variabilities in the observed $PM_{2.5}$ concentration during 2014–2023 ($0.59 \mu\text{g m}^{-3}$, $P < 0.01$). In Europe, the 2023 Canadian wildfires contributed to an average of $0.43 \mu\text{g m}^{-3}$ annual mean $PM_{2.5}$ over the locations of European Environment Agency (EEA) sites, accounting for 20% of the differences in observed $PM_{2.5}$ concentration between 2022 and 2023 ($2.10 \mu\text{g m}^{-3}$) and 14% of the mean interannual variabilities in observed $PM_{2.5}$ concentration during 2014–2023 ($3.02 \mu\text{g m}^{-3}$, $P < 0.05$).

Long-range transport of the 2023 Canadian wildfire plumes to Europe

The Hybrid Single-Particle Lagrangian Integrated Trajectory (HYSPLIT) model has been widely used to track the back trajectories for air parcels arriving at the receptor^{101–104}. To track the transports and sources of $PM_{2.5}$ pollution in Europe related to the 2023 Canadian wildfires, we used the HYSPLIT model to calculate the 7-day back trajectories for the entire European region (excluding Russia) on a $0.1^\circ \times 0.1^\circ$ grid basis from May to September in 2023 at an hourly resolution. The HYSPLIT model version 5.3.0 (<https://www.ready.noaa.gov/ready2-bin/getlinux-trial.pl/>) was used for the analysis. Each backward trajectory was run for 7 days with 1-hour time steps, initialized at 0:00, 6:00, 12:00 and 18:00 coordinated universal time (UTC) daily. The arrival height was 500 m above ground, approximately within the planetary boundary layer. The HYSPLIT model was driven by three-dimensional meteorological fields from the Global Data Assimilation System of National Centers for Environmental Prediction (GDAS NCEP), with a time resolution of 3 hours, a horizontal resolution of $1^\circ \times 1^\circ$ and a vertical resolution of 23 levels.

We then defined the transport trajectory density (TTD) to represent the capability of pollutant transport from source regions to the receptor region (Europe), which is the total number of trajectories passing through the $0.1^\circ \times 0.1^\circ$ grid box of source regions during the study period. The TTD of each grid box during the study period can be calculated by equation (13):

$$\text{TTD}_i = \sum_{j=1}^m F_{i,j} \quad (13)$$

where i is the index of each grid box and m is the total number of trajectories that passed through all receptor grid boxes (81,052 in this study). For each trajectory j (ranging from 1 to m), $F_{i,j}$ is defined as 1 if trajectory j passes through grid box i ; otherwise, $F_{i,j}$ is defined as 0. Therefore, TTD _{i} is the total number of trajectories that passed through the grid box i during the study period. Supplementary Fig. 9 shows the spatial distribution of TTD sums from May to September in 2023. High TTD values were observed over the majority of Canada between May and September 2023, indicating the frequent trans-Atlantic plumes that prompt pollution transported from the wildfire source regions to downwind regions, and finally reached Europe.

Supplementary Fig. 10 further illustrates the vertical transport process that brought the Canadian wildfire plumes to the surface of Europe during the late-June trans-Atlantic episode. High $PM_{2.5}$ concentrations are observed on 29 June and 2 July over the large areas in Northern France and Belgium (Supplementary Fig. 8 and Supplementary Fig. 10a). During the pollution episode, the GEOS-Chem simulation shows that the enhancement of surface $PM_{2.5}$ concentration from Canadian wildfires was accompanied by a high $PM_{2.5}$ concentration at high altitude (Supplementary Fig. 10b). The modelled $PM_{2.5}$ enhancement from Canadian wildfires corresponds well with the observed peak of $PM_{2.5}$ concentration, demonstrating the vertical transport process during the episode. Meanwhile, 7-day back trajectories with 500-m arrival height indicate that the airflows originating from the Canadian wildfire source regions were transported into the boundary layer above the site location on 29 June and 2 July (Supplementary Fig. 10c), providing compelling evidence of long-range transport of wildfire-related $PM_{2.5}$ from Canada to Europe.

Health impacts

Acute mortality attributable to exposure to Canadian wildfires.

The acute and chronic mortality attributable to 2023-Canadian-wildfires-related PM_{2.5} exposure were estimated separately. The acute mortality was estimated for all grids 'Canada smoke days' in which both (1) grid daily mean PM_{2.5} concentrations exceeded 15 µg m⁻³ (the recommended 24-hour average guideline levels of the WHO) and (2) Canadian-wildfires-related PM_{2.5} accounted for at least half of the total daily PM_{2.5} (ref. 10). Details on the estimation of fire-specific PM_{2.5} concentrations are described above. Following previous studies⁵⁰, the acute mortality attributable to Canadian wildfires PM_{2.5} exposure was assessed using equation (14):

$$D_{i,j} = \sum_{j=1}^{365} \{[(RR(C_{i,j}) - 1)/RR(C_{i,j})] \times P_i \times (I_i(\text{Country}_a)/365)\} \quad (14)$$

where $D_{i,j}$ represents the all-cause acute premature mortality attributable to Canadian-wildfires-related PM_{2.5} exposure in grid i on day j . $RR(C_{i,j})$ represents the relative risk at exposure level C in grid i on day j and the exposure level was assessed as the daily average Canadian-wildfires-related PM_{2.5} concentrations. A global RR estimates of 1.021 (95% CI, 1.018, 1.024)¹⁵ per 10 µg m⁻³ increase of wildfire PM_{2.5} exposure was used for all regions. P_i represents the population in grid i that was constructed as described in 'Estimation of fire-specific PM_{2.5} exposure'. I_i represents the baseline all-cause death rate in grid i that belong to Country a , which was collected from the Global Burden of Disease (GBD) 2019 study (<https://ghdx.healthdata.org/gbd-2019>)⁴⁵.

Compelling evidence for the increased toxicity of wildfire-related PM_{2.5} relative to all-source PM_{2.5} have been reported^{13,58}, and various exposure-response functions for acute exposure to wildfire PM_{2.5} have been developed by recent studies^{15,46,48,49}. Here we use a widely used global pooled relative risk of wildfire PM_{2.5} exposure¹⁵ to estimate the acute premature mortality considering the global nature of this study and the comparability across different regions. To investigate the impacts of the choice of relative risks on the acute premature mortality estimates, we further assess the acute premature mortality attributable to the 2023 Canadian wildfires by using the relative risks for wildfire PM_{2.5} from newly developed global meta-analysis⁴⁶, two studies in North America^{48,49} and relative risk from a meta-analysis on all-source PM_{2.5} (ref. 50). The results of comparison are presented in Supplementary Table 7. The estimated global acute premature mortality attributable to Canada smoke day exposure varied by a factor of four when different RR estimates were used. Among the different functions derived for wildfire PM_{2.5}, mortality estimates using global pooled relative risks^{15,46} (ranging from 2,800 to 5,400) were higher than those using regional relative risks^{48,49} (1,300–2,600). Estimates using relative risks derived for wildfire PM_{2.5} exposure^{15,46,48,49} generally yield higher mortality estimates (1,300–5,400) than those using all-source relative risk⁵⁰ (1,800), implying increased toxicity of wildfire-related PM_{2.5} compared with all-source PM_{2.5}.

Chronic premature mortality attributable to exposure to Canadian wildfires.

All-cause premature mortality attributable to chronic smoke exposure from the 2023 Canadian wildfires was estimated with a meta-analysis relative risk estimate of 1.08 (95% CI, 1.06, 1.09) per 10 µg m⁻³ increase in PM_{2.5} exposure⁴⁰.

The health burden attributable to chronic PM_{2.5} exposure was assessed using equation (15):

$$D_i = [(RR(C_i) - 1)/RR(C_i)] \times P_i \times I_i(\text{Country}_a) \quad (15)$$

where $D_{y,i,n}$ represents the chronic premature mortality attributable to Canadian-wildfires-related PM_{2.5} exposure in grid i . $RR(C_i)$ represents the relative risk at exposure level C in grid i . C_i represents the annual average PM_{2.5} concentration in grid i . P_i represents the population in

grid i , and I_i represented the baseline all-cause death rate in grid i in Country a of year 2019, which was collected from the GBD 2019 study (<https://ghdx.healthdata.org/gbd-2019>)⁴⁵. The theoretical minimum risk exposure level (TMREL) for the chronic health effects attributable to PM_{2.5} ranged between 2.4 µg m⁻³ and 5.9 µg m⁻³, as reported in the GBD 2019 study.

The chronic exposure mortality attributable to Canadian wildfires was assessed with the direct proportion approach^{105,106}, which assumes that the increase in mortality is in proportion to the increases in PM_{2.5} exposure. Thus, the chronic exposure mortality attributable to all-source ambient PM_{2.5} exposure was assessed first and the Canadian-wildfires-associated chronic mortality was quantified by calculating the proportion of Canadian-wildfire-derived PM_{2.5} within all-source ambient PM_{2.5}.

It should be noted that the RR used here is derived for all-source PM_{2.5} rather than wildfire PM_{2.5}, owing to the limited epidemiological evidence of chronic health effects from wildfire-related PM_{2.5} exposure. We use the exposure-response function for all-cause mortality rather than the cause-specific exposure-response function (that is, the widely used GBD approach⁴⁵) as this study aims to estimate the total mortality burden whereas the cause-specific may underestimate the total chronic mortality of ambient PM_{2.5} (ref. 107). Relative risk derived from regional meta-analysis^{47,49} may differ from those derived from global pooled analysis⁴⁰. Given the global nature of this study, we choose the all-cause global pooled relative risk in our analysis⁴⁰. We further conducted a sensitivity analysis to evaluate the impact of exposure-response functions on the chronic premature mortality^{45,47,49}, as shown in Supplementary Table 8. Using cause-specific exposure-response function⁴⁵ yields 31,000 global chronic premature mortality, lower than estimates using all-cause functions^{40,47,49} (ranging from 82,100 to 152,000). For all-cause premature mortality estimates with 3 different relative risks, mortalities estimated by global relative risk⁴⁰ (82,100) are remarkably lower than those estimated by regional relative risks^{47,49} (that is, the USA, 117,500–152,000), indicating large variation of relative risks across different global regions.

We also reviewed the approaches of estimating chronic health burden from wildfire-related PM_{2.5} exposure used in different global and regional studies^{12,31,44,46,108–123}, as shown in Supplementary Table 9. Although annual average exposure is widely used in those studies, it may not reflect the population experience of sporadic wildfire PM_{2.5} exposure owing to the different nature of wildfire smoke exposure and the urban and background pollution exposure. Substantial differences in chronic health burden assessment approaches were observed, which varied in mortality endpoints (cause-specific versus all-cause), the relative risk and the definition of exposed population. Many of those studies quantified PM_{2.5}-related health impacts of landscape fires on populations that are annually impacted by fire-related air pollution from local or nearby fires, whereas our study investigated the transboundary air pollution and the health burden of a single extreme wildfire event. Specifically, ref. 31 quantified the transboundary PM_{2.5} health impact of wildfires in the Arctic Council, which is most comparable to the purpose of our study. In their analysis, areas where the increase in carbonaceous PM_{2.5} from wildfires was statistically insignificant were excluded from the health impact assessment. A previous study⁴⁶ estimated global, regional, and national mortality burden attributable to fire-related PM_{2.5} exposure, which is estimated for all population with the same exposure-response function used in our study⁴⁰. We then followed the widely accepted approach in our analysis and conducted significance tests for the estimated contribution of the annual mean PM_{2.5} concentration from the 2023 Canadian wildfires.

Uncertainty analysis

Our results are subject to a number of uncertainties and limitations. The uncertainty ranges (95% CI) in different steps of our analysis are discussed below.

First, the emission inventories used in this study bear large uncertainties. For example, the uncertainties in the GFED emissions mainly come from the inadequate representation of the natural variation of the emission factors during fire events, and the high uncertainties in the amount of fuel burned estimated from burned area. It is reported that a best-guess uncertainty assessment for GFEDv4.1s at regional scales could be a 1σ of about 50% in general but higher in areas where small fires burned area is important or where there is notable fuel consumption in organic soils³⁷.

Second, the PM_{2.5} concentrations simulated by the global chemical transport model are affected by errors in emission inventories and the model's representation of physical and chemical processes such as vertical transport⁵¹ and secondary organic aerosols¹²⁴. Specifically, the smoke-injection height is not considered in the GEOS-Chem simulation, which may lead to overestimates and underestimates of fire-related PM_{2.5} concentrations in fire source regions and downwind regions, respectively⁵¹. Given the huge computational cost for model sensitivity simulations considering the uncertainties in emissions, we use the normalized root-mean-square deviation (NRMSD) between the modelled and the observed PM_{2.5} concentrations to represent the overall model errors in total PM_{2.5}, and use the NRMSD between the modelled and the observed PM_{2.5} concentrations over fire events to represent the model errors in fire-related PM_{2.5}. The NRMSD for GEOS-Chem-based total PM_{2.5} and fire-related PM_{2.5} ranged between 42.8% and 62.0% and between 44.3% and 53.0%, respectively, among Canada, the USA and Europe, but a bit higher in other regions globally (for example, close to 100.0%). Although the absolute errors in GEOS-Chem-based simulations are large, some errors are common between the total and fire-related PM_{2.5} and have limited impacts on their ratios.

Third, the multi-source fused PM_{2.5} data obtained from our retrieval model are influenced by errors in all the input data and the multilayer machine-learning model itself. We have fully evaluated the model's performance using a cross-validation approach and the performance was comparable to previous studies^{10,41}. We use the NRMSD between PM_{2.5} retrieval and observed PM_{2.5} concentrations to represent its uncertainties (2.0–7.1% among different regions).

As presented in equation (4), the overall uncertainties involved in fire-related PM_{2.5} exposures are determined by uncertainties in GEOS-Chem simulated fractional contributions of fire emissions ($GC_{\text{fire}}/GC_{\text{base}}$) and in total PM_{2.5} exposures based on the retrieval model (C_{PM}). The errors in GC_{base} , GC_{fire} and C_{PM} are defined above. The errors in the ratio ($GC_{\text{fire}}/GC_{\text{base}}$) were then quantified by 10,000 trials of Monte Carlo simulation. Finally, the overall uncertainties of fire-related PM_{2.5} (C_{fire}) were derived from the aggregations of errors above.

The overall uncertainties (presented as 95% CI) of acute and chronic mortality attributable to Canadian wildfires were then assessed by Monte Carlo simulations with 1,000 iterations⁴⁵. Uncertainties embedded in all input parameters of the risk assessment model were considered. The uncertainties in exposure levels are described above. The uncertainties in baseline mortality, exposure–response functions and TMREL were collected from the GBD 2019 study. The uncertainty in national total population was provided by United Nations data (high-fertility and low-fertility scenarios). All the parameters, except TMREL, which was simulated by a uniform distribution, were simulated by normal distributions.

Comparison with other relevant studies

The impacts of the 2023 Canadian wildfires on surface PM_{2.5} air quality have been reported in a few recent studies. By proposing a multidimensional air pollution correlation network framework, ref. 28 argued that the 2023 Canadian wildfires significantly impact the air pollution behaviour in the Northeastern USA region. Reference 29 estimated the PM_{2.5} concentration in the Northeastern USA in June 2023 by combining chemical transport model results and surface PM_{2.5} measurements. They identified two 'smoke wake' events in June 2023 (6–8 June and

28–30 June) with significant PM_{2.5} enhancement caused by the transport of Canadian wildfire plumes. Our results also capture these two events in the same region, although our estimates of PM_{2.5} concentrations are lower than those of ref. 29 during the first 'smoke wave' event (6–8 June), which might be attributed to the coarse model resolution in our analysis (Supplementary Table 3). By using a global chemical transport model, ref. 2 found that the Canadian wildfires significantly impacted air quality in the Northern Hemisphere, which was consistent with our findings. They identified six widespread air pollution episodes due to the Canadian wildfires from May to August, which are also captured in our GESO-Chem simulation (Supplementary Fig. 11) and retrieved PM_{2.5} concentration (Supplementary Fig. 12).

Canadian wildfire-related chronic PM_{2.5} exposure is associated with approximately 22, 10 and 3 deaths per 100,000 people in 2023 in Canada, the USA and Europe, respectively. For comparison, chronic mortalities from all-source PM_{2.5} exposure are 55, 57 and 80 per 100,000 people in 2023 in the three regions, respectively, underscoring the non-negligible contribution of wildfire smoke to public health burdens. Our estimates on Canadian wildfire-related per capita mortality rates in the USA and Canada are notably higher than wildfire-related per capita mortality rates reported in refs. 46,125, owing to high PM_{2.5} exposure levels attributable to the record-breaking Canadian wildfires in 2023 as well as the all-cause exposure–response function used in our analysis.

We estimated that the 2023 Canadian fires accounted for 3.82 μg m⁻³ (3.00–4.64 μg m⁻³) of annual mean PM_{2.5} exposure in Canada in 2023, which is lower than 2000–2019 annual mean fire-related PM_{2.5} exposure in typical wildfire hotspot regions¹⁰ such as sub-Saharan Africa (6.99 μg m⁻³), mainland Southeast Asia (5.77 μg m⁻³), Indonesia (6.28 μg m⁻³) and Brazil (5.68 μg m⁻³). In another study⁴⁴, annual mean fire-related PM_{2.5} exposure in typical wildfire hotspot regions were estimated to be 0.72 μg m⁻³ in Indonesia, 1.26 μg m⁻³ in Brazil and 1.26 μg m⁻³ in Southeast Asia in 2017, indicating the large interannual variabilities in wildfire activities. Reference 109 estimated that global landscape fires alone result in 44 million and 4 million people annually being exposed to air quality considered 'unhealthy' and 'hazardous', respectively. In comparison, we estimated that the 2023 Canadian wildfires caused 139.3 million and 0.25 million people to be exposed to 'unhealthy' (PM_{2.5} > 55 μg m⁻³) and 'hazardous' (PM_{2.5} > 250.5 μg m⁻³) air quality. Large health impacts from wildfire-related air pollution have been reported in these hotspot regions^{46,109–112,114–116,118}. For instance, wildfires-induced chronic mortality was estimated to be 160,200 in Africa in 2017¹¹⁰, 59,000 in Southeast Asia in 2014¹¹⁸, 13,700–44,000 in equatorial Asia during 2004–2015¹¹⁶, and 16,800 in South America in 2012¹¹¹. In recent study⁴⁶, it was estimated that 384,600, 144,300 and 79,300 people died annually in sub-Saharan Africa, Southeast Asia, and Latin American and the Caribbean, respectively, owing to chronic wildfire smoke exposure during 2000–2019. In contrast, we estimated that the 2023 Canadian fires resulted in 8,300 (95% CI, 5,800–10,800) PM_{2.5}-attributable chronic premature deaths in Canada given the low population density close to fire regions. Globally, we estimated 82,100 (95% CI, 47,700–116,500) PM_{2.5}-attributable chronic premature deaths owing to smoke exposure from the 2023 Canadian wildfires, indicating the large health impacts from long-range transported PM_{2.5} pollution.

Although notable impacts of the 2023 Canadian wildfires on surface PM_{2.5} concentration in Europe are observed, those impacts are remarkably low compared with the impact of smoke from local fires that are not diluted by long-range transport. For instance, ref. 126 estimated that 2.1 million people were exposed to concentrations above 36 μg m⁻³ for at least 1 day between 23 and 30 June owing to the Saddleworth Moor and Winter Hill fires in northern England. In comparison, our estimates shows that 0.81 million people in Europe were exposed to the same level of PM_{2.5} pollution for at least 1 day between 26 June and 7 July 2023 owing to the trans-Atlantic pollution of Canadian wildfires.

Dust has been recognized as another important natural source of air pollution^{44,127}. A study¹²⁷ estimated that Sahara dust contributed

5–20 $\mu\text{g m}^{-3}$ of surface PM_{10} concentration in South Europe and 0.5–1.0 $\mu\text{g m}^{-3}$ in North Europe during 2016–2017. Another study⁴⁴ estimated that windblown dust increased the annual mean $\text{PM}_{2.5}$ exposure in 2017 by 1.72 $\mu\text{g m}^{-3}$, 1.50 $\mu\text{g m}^{-3}$, 1.18 $\mu\text{g m}^{-3}$, 0.07 $\mu\text{g m}^{-3}$ and 0.19 $\mu\text{g m}^{-3}$ in Central Europe, Eastern Europe, Western Europe, Canada and the USA, respectively. $\text{PM}_{2.5}$ exposure was lower than dust-related $\text{PM}_{2.5}$ exposure in Europe but higher than that in Canada and the USA. In turn, windblown dust contributed to 34,972, 33 and 1,126 annual chronic premature deaths in Europe, Canada and the USA, respectively⁴⁴. Our estimates for Canadian-wildfire-related deaths are substantially lower than dust-related deaths in Europe, but much higher than that in Canada and the USA. It should be noted that both dust and fire activities have large interannual variabilities so the comparison could be different for other years.

Data availability

GFEDv4.1s emission data are available at <https://surfdrive.surf.nl/files/index.php/s/5y7TdE6ufwpkAW1>. QFEDv2.5r1 emission data are available at <https://portal.nccs.nasa.gov/datashare/gmao/qfed/>. GFASv1.2 data are available at <https://ads.atmosphere.copernicus.eu/cdsapp#!/dataset/cams-global-fire-emissions-gfas?tab=overview/>. $\text{PM}_{2.5}$ surface monitoring data for different regions are available from Environmental Canada (<https://data-donnees.az.ec.gc.ca/data/air/monitor/national-air-pollution-surveillance-naps-program/Data-Donnees/>), the US Environmental Protection Agency (US EPA) AirNow (<https://www.epa.gov/outdoor-air-quality-data/download-daily-data>), US EPA Interagency Monitoring of Protected Visual Environments (IMPROVE) (<https://views.cira.colostate.edu/fed/QueryWizard/Default.aspx>), the US Forest Service (<https://info.airfire.org/airmonitor-package>), the European Air Quality Portal (<https://eadmz1-cws-wp-air02.azurewebsites.net/>), the China National Environmental Monitoring Center (CNEMC, <http://www.cnemc.cn/>), and OpenAQ (<https://openaq.org/>). Satellite AOD retrievals from the MODIS Level 2 aerosol products (MOD04 and MYD04) are available at <https://ladsweb.modaps.eosdis.nasa.gov/search/>. The CAMS modelling and reanalysis data are available at <https://ads.atmosphere.copernicus.eu>. The smoke plume information from the Hazard Mapping System (HMS) is available at <https://www.ospo.noaa.gov/Products/land/hms.html>. The GEOS-FP reanalysis data are available at <https://portal.nccs.nasa.gov/datashare/gmao/geos-fp/>. The WorldPop gridded global population distribution data can be obtained from <https://www.worldpop.org/>. The national total population data of each year are from United Nations (<https://population.un.org/wpp/>), US Census Bureau, Population Division (<https://www.census.gov/data/tables/time-series/demo/popest/2020s-state-total.html>) and Statistics Canada (<https://www150.statcan.gc.ca/>). The baseline national all-cause death rate, cause-specific death rate, and 5-year age-specified population structure from the GBD study can be obtained from <https://vizhub.healthdata.org/gbd-results/>. Global fire-related $\text{PM}_{2.5}$ concentration in 2023 generated from this study is available from the figshare repository at <https://doi.org/10.6084/m9.figshare.25736643.v1> and <http://tapdata.org.cn>. All maps were created based on freely available shapefiles from the Database of Global Administrative Boundaries (<https://gadm.org/>), using NCAR Command Language (NCL) v6.4.0 (<http://www.ncl.ucar.edu/>) and R v4.1.3 (<https://www.r-project.org/>) with the ggplot2 v3.5.1 (<https://ggplot2.tidyverse.org>) library. All data presented in the paper are provided with this paper. Source data are provided with this paper.

Code availability

GEOS-Chem 14.0.1 used in this study is available at <https://zenodo.org/records/7271974> (ref. 128). The code developed for this study is available from <https://github.com/QingyangXiao/Code-for-calculating-global-fire-related-PM2.5-and-health-impacts>.

65. Randerson, J. T., Van Der Werf, G. R., Giglio, L., Collatz, G. J. & Kasibhatla, P. S. *Global Fire Emissions Database, Version 4.1 (GFEDv4)* (ORNL DAAC, 2018).
66. Giglio, L., Randerson, J. T. & Van Der Werf, G. R. Analysis of daily, monthly, and annual burned area using the fourth-generation Global Fire Emissions Database (GFED4). *J. Geophys. Res. Biogeosci.* **118**, 317–328 (2013).
67. Randerson, J. T., Chen, Y., van der Werf, G. R., Rogers, B. M. & Morton, D. C. Global burned area and biomass burning emissions from small fires. *J. Geophys. Res. Biogeosci.* **117**, G04012 (2012).
68. Akagi, S. K. et al. Emission factors for open and domestic biomass burning for use in atmospheric models. *Atmos. Chem. Phys.* **11**, 4039–4072 (2011).
69. Randles, C. A. et al. The MERRA-2 aerosol reanalysis, 1980 onward. Part I: System description and data assimilation evaluation. *J. Clim.* **30**, 6823–6850 (2017).
70. Lu, X. et al. Wildfire influences on the variability and trend of summer surface ozone in the mountainous western United States. *Atmos. Chem. Phys.* **16**, 14687–14702 (2016).
71. Liu, J. C. et al. Wildfire-specific fine particulate matter and risk of hospital admissions in urban and rural counties. *Epidemiology* **28**, 77–85 (2017).
72. Wang, S. C. et al. Transport of Central American fire emissions to the U.S. Gulf Coast: climatological pathways and impacts on ozone and $\text{PM}_{2.5}$. *J. Geophys. Res. Atmos.* **123**, 8344–8361 (2018).
73. Lutsch, E. et al. Detection and attribution of wildfire pollution in the Arctic and northern midlatitudes using a network of Fourier-transform infrared spectrometers and GEOS-Chem. *Atmos. Chem. Phys.* **20**, 12813–12851 (2020).
74. Xue, T. et al. Open fire exposure increases the risk of pregnancy loss in South Asia. *Nat. Commun.* **12**, 3205 (2021).
75. Wizenberg, T. et al. Exceptional wildfire enhancements of PAN, C_2H_4 , CH_3OH , and HCOOH over the Canadian High Arctic during August 2017. *J. Geophys. Res. Atmos.* **128**, e2022JD038052 (2023).
76. Wu, Y. et al. Wildfire-related $\text{PM}_{2.5}$ and health economic loss of mortality in Brazil. *Environ. Int.* **174**, 107906 (2023).
77. Rienecker, M. M. et al. *The GEOS-5 Data Assimilation System-Documentation of Versions 5.0.1, 5.1.0, and 5.2.0*. Report No. NASA/TM-2008-104606 (NASA, 2008).
78. Fountoukis, C. & Nenes, A. ISORROPIA II: a computationally efficient thermodynamic equilibrium model for K^+ – Ca^{2+} – Mg^{2+} – NH_4^+ – Na^+ – SO_4^{2-} – NO_3^- – Cl^- – H_2O aerosols. *Atmos. Chem. Phys.* **7**, 4639–4659 (2007).
79. Lin, H. P. et al. Harmonized Emissions Component (HEMCO) 3.0 as a versatile emissions component for atmospheric models: application in the GEOS-Chem, NASA GEOS, WRF-GC, CESM2, NOAA GEFS-Aerosol, and NOAA UFS models. *Geosci. Model Dev.* **14**, 5487–5506 (2021).
80. McDuffie, E. E. et al. A global anthropogenic emission inventory of atmospheric pollutants from sector- and fuel-specific sources (1970–2017): an application of the Community Emissions Data System (CEDS). *Earth Syst. Sci. Data* **12**, 3413–3442 (2020).
81. Simone, N. W., Stettler, M. E. J. & Barrett, S. R. H. Rapid estimation of global civil aviation emissions with uncertainty quantification. *Transp. Res. Part D* **25**, 33–41 (2013).
82. Fairlie, T. D., Jacob, D. J. & Park, R. J. The impact of transpacific transport of mineral dust in the United States. *Atmos. Environ.* **41**, 1251–1266 (2007).
83. Jaeglé, L., Quinn, P. K., Bates, T. S., Alexander, B. & Lin, J. T. Global distribution of sea salt aerosols: new constraints from in situ and remote sensing observations. *Atmos. Chem. Phys.* **11**, 3137–3157 (2011).
84. Murray, L. T., Jacob, D. J., Logan, J. A., Hudman, R. C. & Koshak, W. J. Optimized regional and interannual variability of lightning in a global chemical transport model constrained by LIS/OTD satellite data. *J. Geophys. Res. Atmos.* **117**, D20307 (2012).
85. Hudman, R. C. et al. Steps towards a mechanistic model of global soil nitric oxide emissions: implementation and space based-constraints. *Atmos. Chem. Phys.* **12**, 7779–7795 (2012).
86. Guenther, A. B. et al. The Model of Emissions of Gases and Aerosols from Nature version 2.1 (MEGAN2.1): an extended and updated framework for modeling biogenic emissions. *Geosci. Model Dev.* **5**, 1471–1492 (2012).
87. Lin, J. T. & McElroy, M. B. Impacts of boundary layer mixing on pollutant vertical profiles in the lower troposphere: implications to satellite remote sensing. *Atmos. Environ.* **44**, 1726–1739 (2010).
88. Levy, R. C. et al. The Collection 6 MODIS aerosol products over land and ocean. *Atmos. Meas. Tech.* **6**, 2989–3034 (2013).
89. Inness, A. et al. The CAMS reanalysis of atmospheric composition. *Atmos. Chem. Phys.* **19**, 3515–3556 (2019).
90. Schroeder, W. et al. Validation analyses of an operational fire monitoring product: the Hazard Mapping System. *Int. J. Remote Sens.* **29**, 6059–6066 (2008).
91. Wardrop, N. A. et al. Spatially disaggregated population estimates in the absence of national population and housing census data. *Proc. Natl Acad. Sci. USA* **115**, 3529–3537 (2018).
92. Reed, F. J. et al. Gridded population maps informed by different built settlement products. *Data* **3**, 33 (2018).
93. United Nations, Department of Economic and Social Affairs, Population Division. *World Population Prospects 2022: Methodology of the United Nations Population Estimates and Projections*. Report No. UN DESA/POP/2022/TR/NO. 4 (United Nations, 2022).
94. US Census Bureau, Population Division. *Annual Estimates of the Resident Population for the United States, Regions, States, District of Columbia, and Puerto Rico: April 1, 2020 to July 1, 2023*. NST-EST2023-POP (US Census Bureau, 2023).
95. Geng, G. N. et al. Tracking air pollution in China: near real-time $\text{PM}_{2.5}$ retrievals from multisource data fusion. *Environ. Sci. Technol.* **55**, 12106–12115 (2021).
96. Xiao, Q. Y. et al. Separating emission and meteorological contributions to long-term $\text{PM}_{2.5}$ trends over eastern China during 2000–2018. *Atmos. Chem. Phys.* **21**, 9475–9496 (2021).
97. Ma, Z. W. et al. Satellite-based spatiotemporal trends in $\text{PM}_{2.5}$ concentrations: China, 2004–2013. *Environ. Health Perspect.* **124**, 184–192 (2016).
98. Bai, K. X., Li, K., Guo, J. P. & Chang, N. B. Multiscale and multisource data fusion for full-coverage $\text{PM}_{2.5}$ concentration mapping: can spatial pattern recognition come with modeling accuracy? *ISPRS J. Photogramm. Remote Sens.* **184**, 31–44 (2022).

99. Xue, T. et al. Spatiotemporal continuous estimates of PM_{2.5} concentrations in China, 2000–2016: a machine learning method with inputs from satellites, chemical transport model, and ground observations. *Environ. Int.* **123**, 345–357 (2019).
100. Shen, S. et al. Enhancing global estimation of fine particulate matter concentrations by including geophysical a priori information in deep learning. *ACS ES&T Air* **1**, 332–345 (2024).
101. Draxler, R. R. & Hess, G. D. An overview of the HYSPLIT_4 modelling system for trajectories. *Aust. Meteorol. Mag.* **47**, 295–308 (1998).
102. Lu, Z. F., Streets, D. G., Zhang, Q. & Wang, S. W. A novel back-trajectory analysis of the origin of black carbon transported to the Himalayas and Tibetan Plateau during 1996–2010. *Geophys. Res. Lett.* **39**, L01809 (2012).
103. Tang, W. Y. et al. Widespread phytoplankton blooms triggered by 2019–2020 Australian wildfires. *Nature* **597**, 370–375 (2021).
104. Cedeño Laurent, J. G. et al. Physicochemical characterization of the particulate matter in New Jersey/New York City area, resulting from the Canadian Quebec wildfires in June 2023. *Environ. Sci. Technol.* <https://doi.org/10.1021/acs.est.4c02016> (2024).
105. Zhang, Q. et al. Transboundary health impacts of transported global air pollution and international trade. *Nature* **543**, 705–709 (2017).
106. Zhao, H. Y. et al. Reduction of global life expectancy driven by trade-related transboundary air pollution. *Environ. Sci. Technol. Lett.* **9**, 212–218 (2022).
107. Burnett, R. et al. Global estimates of mortality associated with long-term exposure to outdoor fine particulate matter. *Proc. Natl Acad. Sci. USA* **115**, 9592–9597 (2018).
108. Lelieveld, J., Evans, J. S., Fnais, M., Giannadaki, D. & Pozzer, A. The contribution of outdoor air pollution sources to premature mortality on a global scale. *Nature* **525**, 367–371 (2015).
109. Roberts, G. & Wooster, M. J. Global impact of landscape fire emissions on surface level PM_{2.5} concentrations, air quality exposure and population mortality. *Atmos. Environ.* **252**, 118210 (2021).
110. Gordon, J. N. D. et al. The effects of trash, residential biofuel, and open biomass burning emissions on local and transported PM_{2.5} and its attributed mortality in Africa. *GeoHealth* **7**, e2022GH000673 (2023).
111. Butt, E. W. et al. Large air quality and human health impacts due to Amazon forest and vegetation fires. *Environ. Res. Commun.* **2**, 095001 (2020).
112. Nawaz, M. O. & Henze, D. K. Premature deaths in Brazil associated with long-term exposure to PM_{2.5} from Amazon fires between 2016 and 2019. *GeoHealth* **4**, e2020GH000268 (2020).
113. Matz, C. J. et al. Health impact analysis of PM_{2.5} from wildfire smoke in Canada (2013–2015, 2017–2018). *Sci. Total Environ.* **725**, 138506 (2020).
114. Koplit, S. N. et al. Public health impacts of the severe haze in equatorial Asia in September–October 2015: demonstration of a new framework for informing fire management strategies to reduce downwind smoke exposure. *Environ. Res. Lett.* **11**, 094023 (2016).
115. Crippa, P. et al. Population exposure to hazardous air quality due to the 2015 fires in equatorial Asia. *Sci. Rep.* **6**, 37074 (2016).
116. Kiely, L. et al. Air quality and health impacts of vegetation and peat fires in equatorial Asia during 2004–2015. *Environ. Res. Lett.* **15**, 094054 (2020).
117. Barbosa, J. V., Nunes, R. A. O., Alvim-Ferraz, M. C. M., Martins, F. G. & Sousa, S. I. V. Health and economic burden of wildland fires PM_{2.5}-related pollution in Portugal—a longitudinal study. *Environ. Res.* **240**, 117490 (2024).
118. Reddington, C. L. et al. Air pollution from forest and vegetation fires in Southeast Asia disproportionately impacts the poor. *GeoHealth* **5**, e2021GH000418 (2021).
119. Fann, N. et al. The health impacts and economic value of wildland fire episodes in the U.S.: 2008–2012. *Sci. Total Environ.* **610–611**, 802–809 (2018).
120. Ford, B. et al. Future fire impacts on smoke concentrations, visibility, and health in the contiguous United States. *GeoHealth* **2**, 229–247 (2018).
121. O'Dell, K. et al. Estimated mortality and morbidity attributable to smoke plumes in the United States: not just a western US problem. *GeoHealth* **5**, e2021GH000457 (2021).
122. Liu, Y. et al. Health Impact Assessment of the 2020 Washington State wildfire smoke episode: excess health burden attributable to increased PM_{2.5} exposures and potential exposure reductions. *GeoHealth* **5**, e2020GH000359 (2021).
123. Neumann, J. E. et al. Estimating PM_{2.5}-related premature mortality and morbidity associated with future wildfire emissions in the western US. *Environ. Res. Lett.* **16**, 035019 (2021).
124. Liao, H., Henze, D. K., Seinfeld, J. H., Wu, S. L. & Mickley, L. J. Biogenic secondary organic aerosol over the United States: comparison of climatological simulations with observations. *J. Geophys. Res. Atmos.* **112**, D06201 (2007).
125. Ma, Y. et al. Long-term exposure to wildland fire smoke PM_{2.5} and mortality in the contiguous United States. *Proc. Natl Acad. Sci. USA* **121**, e2403960121 (2024).
126. Graham, A. M. et al. Impact on air quality and health due to the Saddleworth Moor fire in northern England. *Environ. Res. Lett.* **15**, 074018 (2020).
127. Wang, Q. Q., Gu, J. W. & Wang, X. R. The impact of Sahara dust on air quality and public health in European countries. *Atmos. Environ.* **241**, 117771 (2020).
128. The International GEOS-Chem User Community. geoschem/GCClassic: GEOS-Chem Classic 14.0.1. *Zenodo* <https://doi.org/10.5281/zenodo.7271974> (2022).

Acknowledgements This work is supported by the National Natural Science Foundation of China (41921005 and 42222507) and the New Cornerstone Science Foundation through the XPLOER PRIZE. We thank G. van der Werf for providing near-real-time GFED4s data and for discussions. We also acknowledge the free use of QFED and GFAS near-real-time fire emission data.

Author contributions Q.Z. conceived of and led the study. Y.W. and Q.Z. conducted the GEOS-Chem simulations and the calculated wildfire-related PM_{2.5}. Q.X., Y.W., Q.Z. and X.L. developed the PM_{2.5} retrieval model and estimated the health impacts. Q.X. and C.H. performed the model evaluation. G.G. and Y.W. conducted the uncertainty analysis. J.Y. performed the back-trajectory analysis. J.L., W.H., B.L., R.V.M., M.B. and J.T.R. provided the analytical tools and data. Q.Z., Y.W., Q.X., G.G., S.J.D. and K.H. interpreted the results. Q.Z., Y.W., Q.X., G.G. and S.J.D. wrote the paper with input from all authors.

Competing interests The authors declare no competing interests.

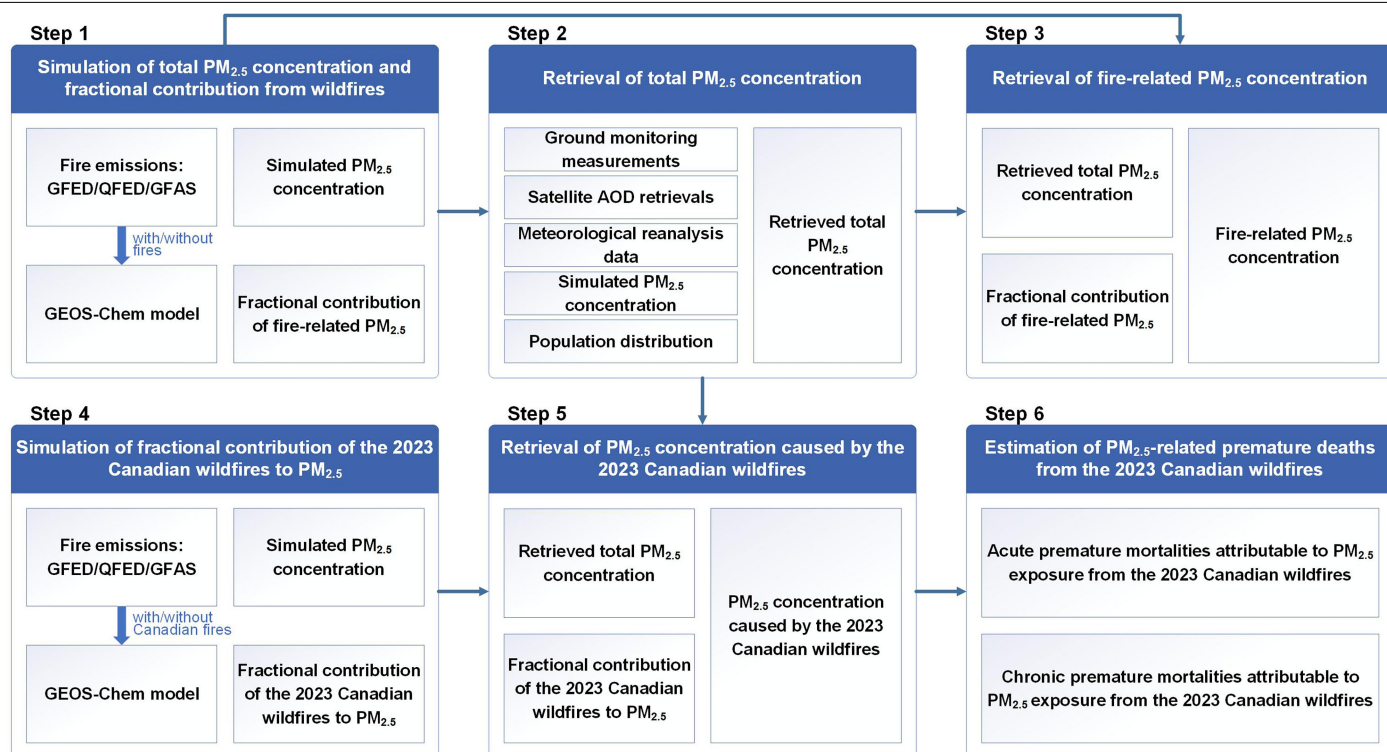
Additional information

Supplementary information The online version contains supplementary material available at <https://doi.org/10.1038/s41586-025-09482-1>.

Correspondence and requests for materials should be addressed to Qiang Zhang.

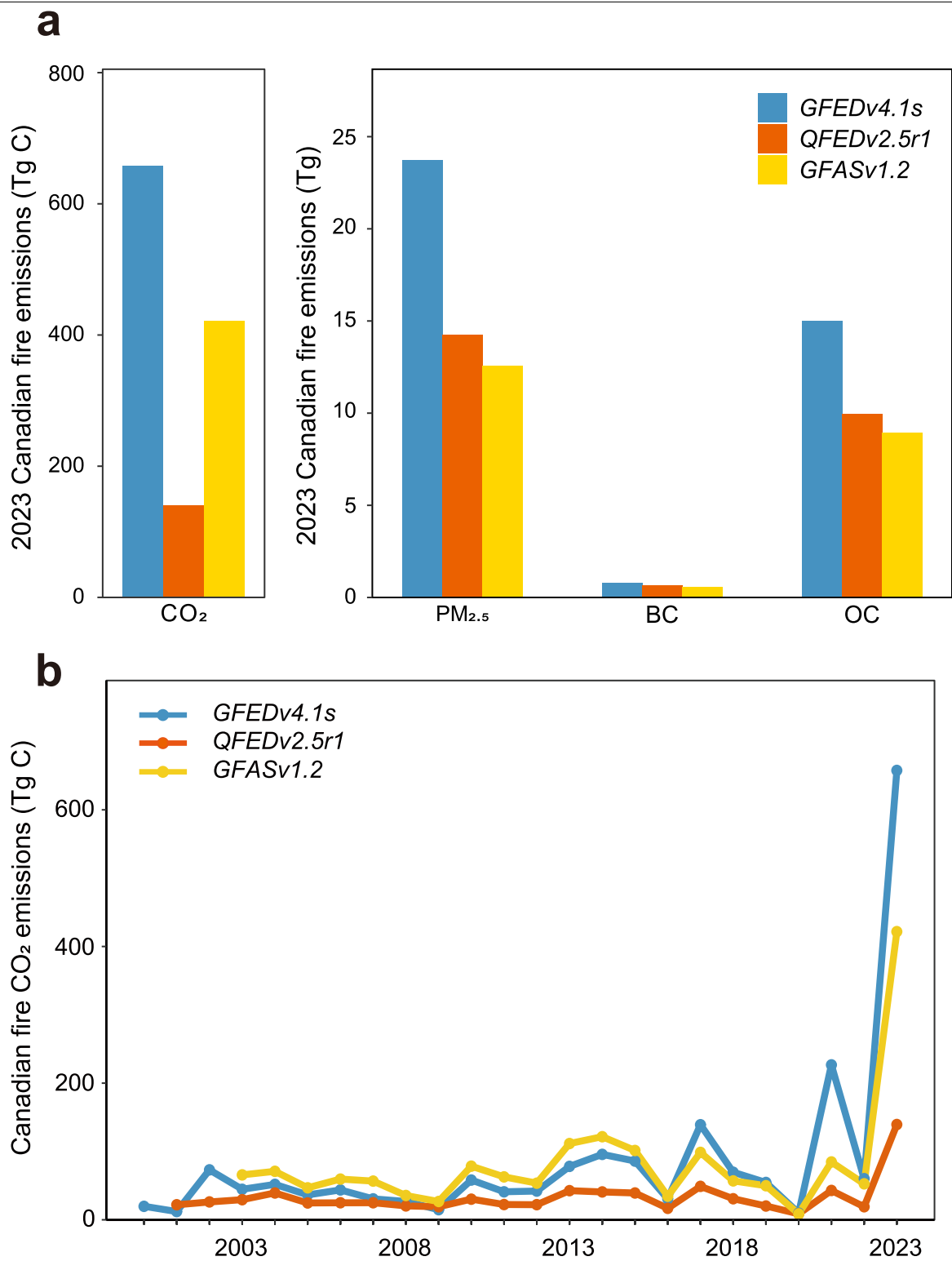
Peer review information Nature thanks the anonymous reviewers for their contribution to the peer review of this work.

Reprints and permissions information is available at <http://www.nature.com/reprints>.



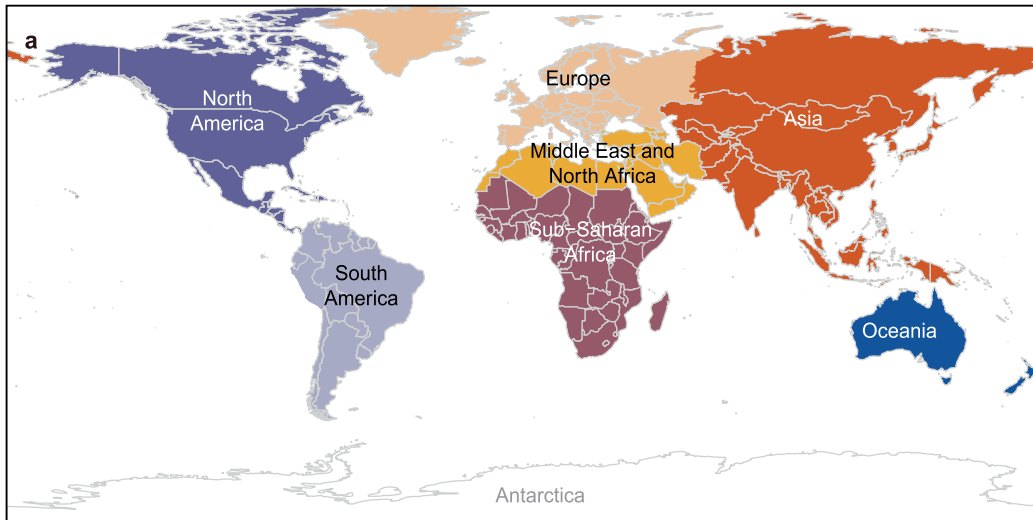
Extended Data Fig. 1 | Methodology framework to estimate $PM_{2.5}$ exposure and mortality attributable to wildfire emissions and from different source regions. The framework comprises six steps: simulation of total $PM_{2.5}$ concentration and fractional contribution from wildfires, retrieval of total $PM_{2.5}$ concentration, retrieval of fire-related $PM_{2.5}$ concentration, simulation

of fractional contribution of the 2023 Canadian wildfires to $PM_{2.5}$ concentration, retrieval of $PM_{2.5}$ concentration caused by the 2023 Canadian wildfires, and estimation of premature deaths attributable to $PM_{2.5}$ exposure from the 2023 Canadian wildfires.

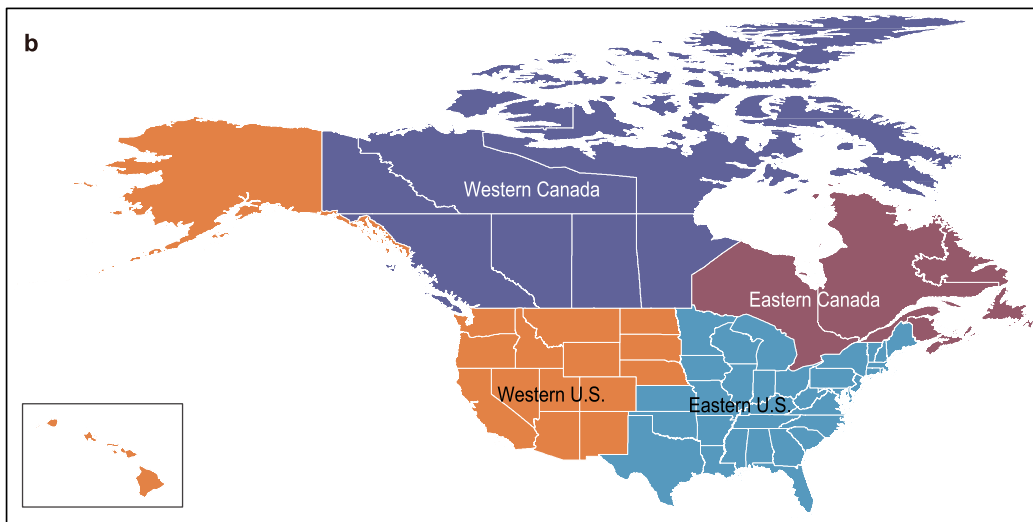


Extended Data Fig. 2 | Canadian wildfire emissions from 2000 to 2023. **a**, Emissions of CO₂ and air pollutants (PM_{2.5}, BC, OC) in 2023. **b**, Annual Canadian wildfire CO₂ emissions from 2000–2023. The bars in **(a)** show the 2023 Canadian wildfire emissions of CO₂ and air pollutants (PM_{2.5}, BC, OC) from GFEDv4.1s (blue), QFEDv2.5r1 (orange) and GFASv1.2 (yellow). The lines in **(b)** show annual Canadian wildfire CO₂ emissions from GFEDv4.1s (blue, 2000–2023), QFEDv2.5r1 (orange, 2001–2023) and GFASv1.2 (yellow, 2003–2023).

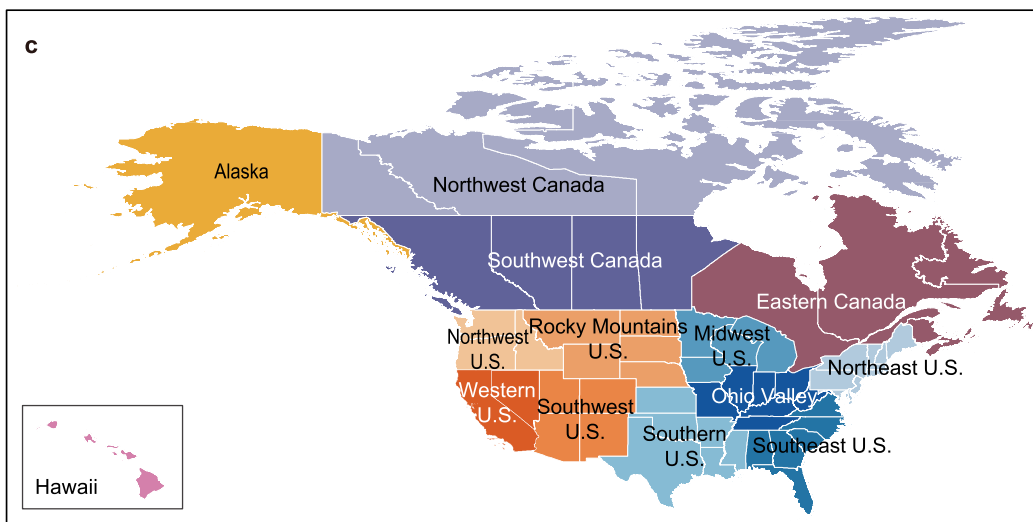
Global region



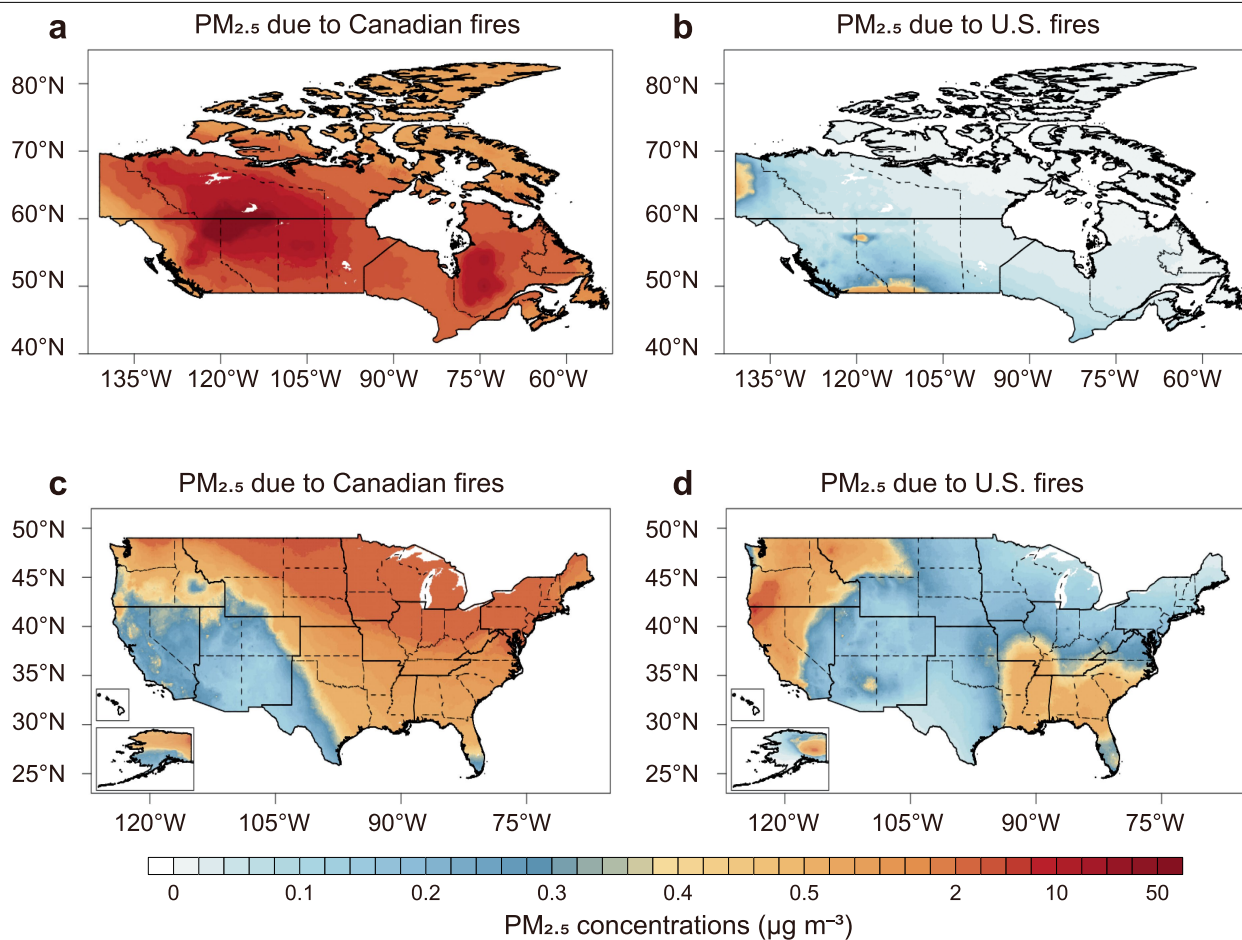
Wildfire source region



Impacted region



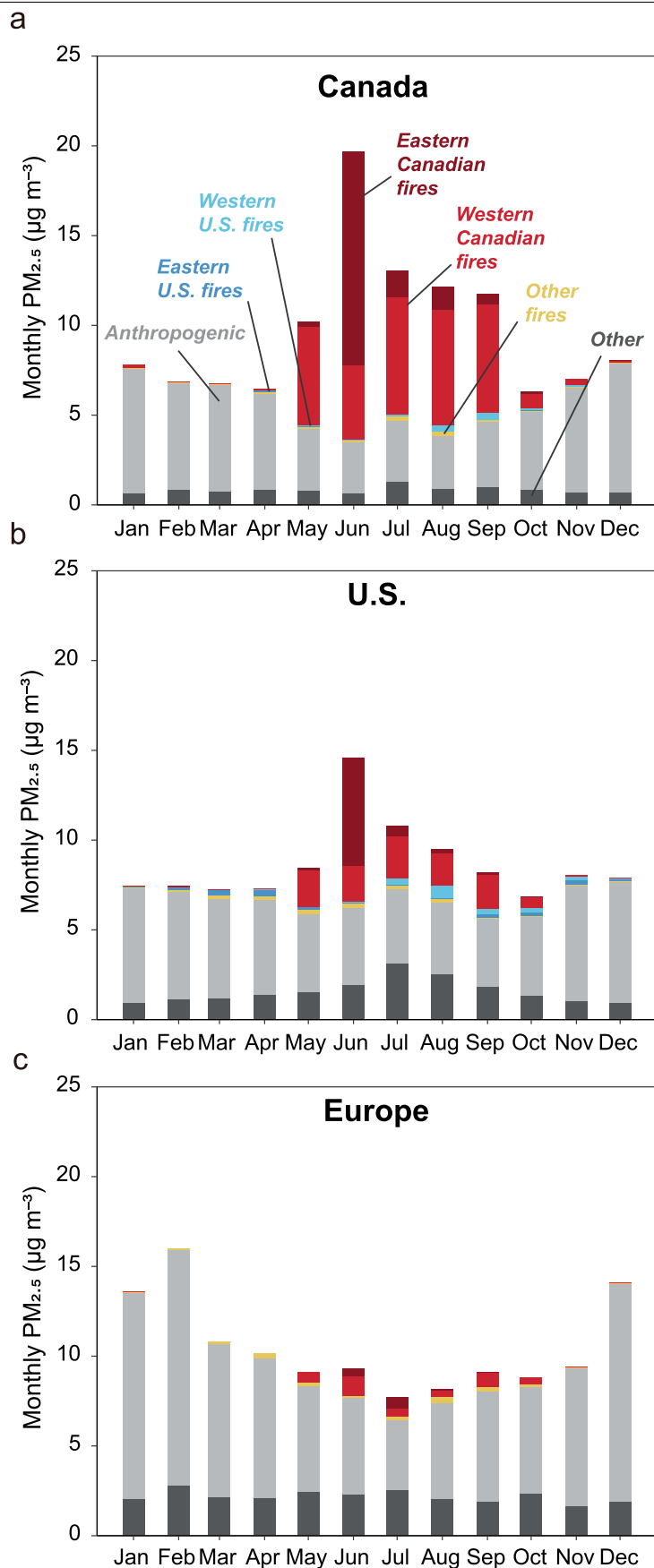
Extended Data Fig. 3 | Region definitions used in this study. **a**, The definitions of the global regions. **b**, The definitions of the wildfire source regions. **c**, The definitions of the impacted regions in North America.

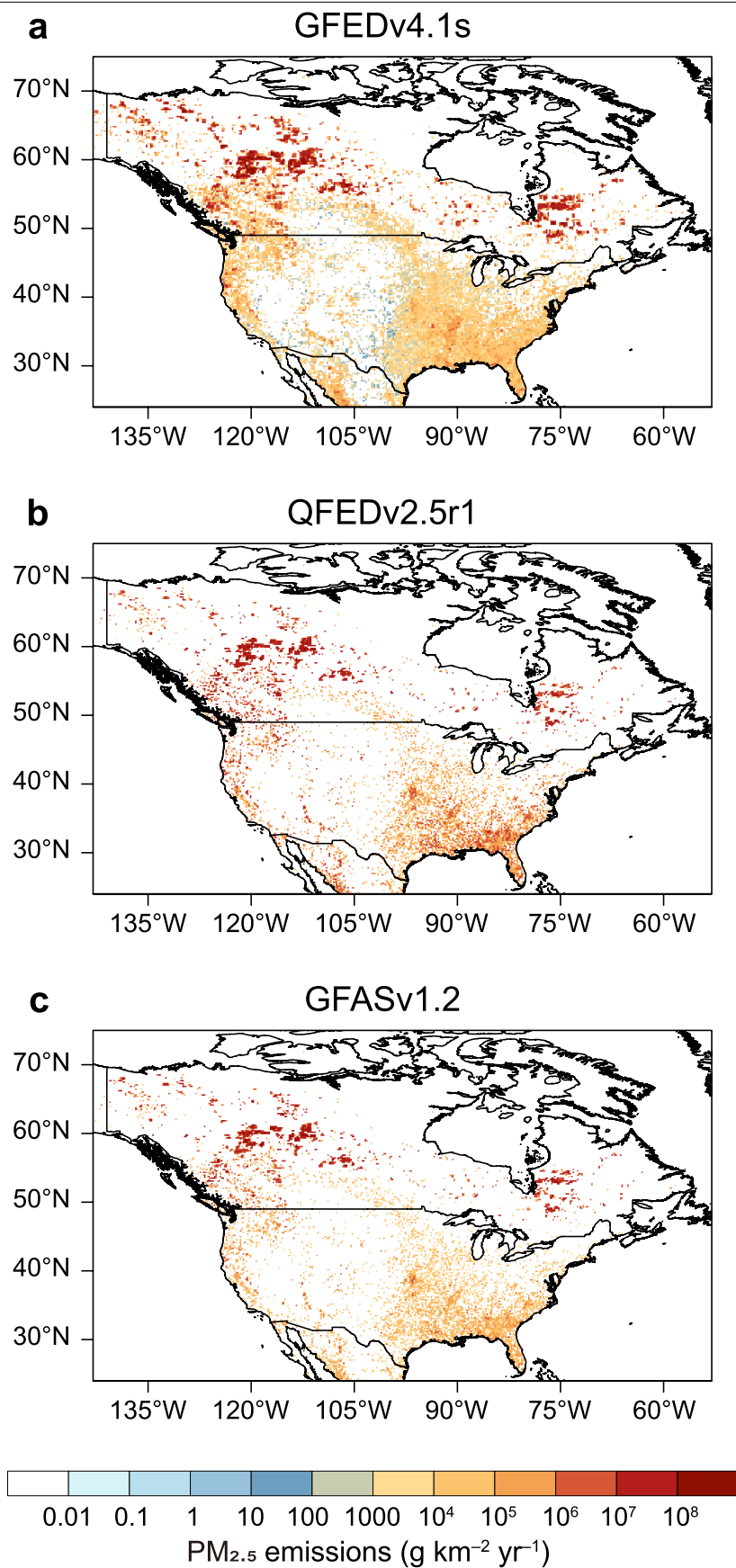


Extended Data Fig. 4 | PM_{2.5} concentration in Canada and U.S. attributable to wildfires in each region. a, b, The 2023 annual mean PM_{2.5} concentrations ($\mu\text{g m}^{-3}$) over Canada related to Canadian fires (a) and the U.S. fires (b).

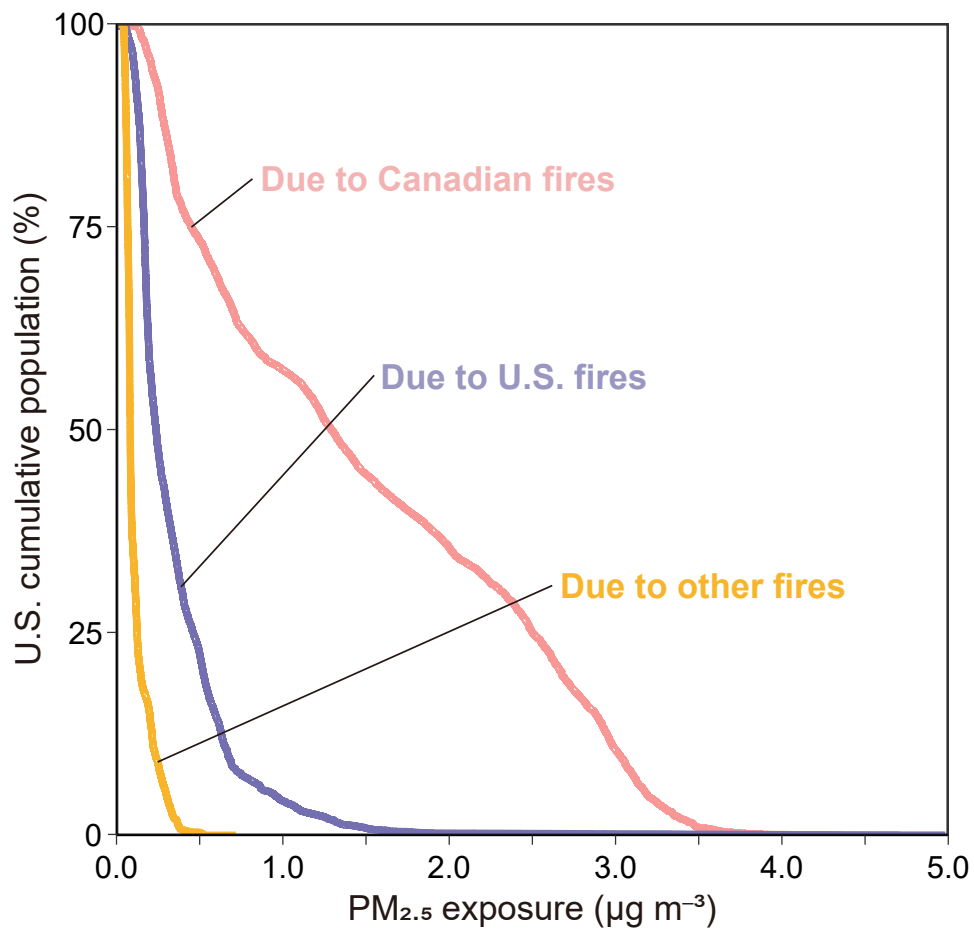
c, d, The 2023 annual mean PM_{2.5} concentrations ($\mu\text{g m}^{-3}$) over the U.S. related to Canadian fires (c) and the U.S. fires (d).

Extended Data Fig. 5 | Monthly PM_{2.5} exposures from different sources in 2023. a,b,c, Monthly PM_{2.5} exposure ($\mu\text{g m}^{-3}$) from wildfires in five source regions (i.e., Eastern Canadian fires, Western Canadian fires, Western U.S. fires, Eastern U.S. fires, and other fires), anthropogenic source, and other sources (including biogenic, dust, and sea salt) in Canada (a), the U.S. (b) and Europe (c) in 2023. In a,b,c, the colors of the stacked bars denote the contribution of the different sources.

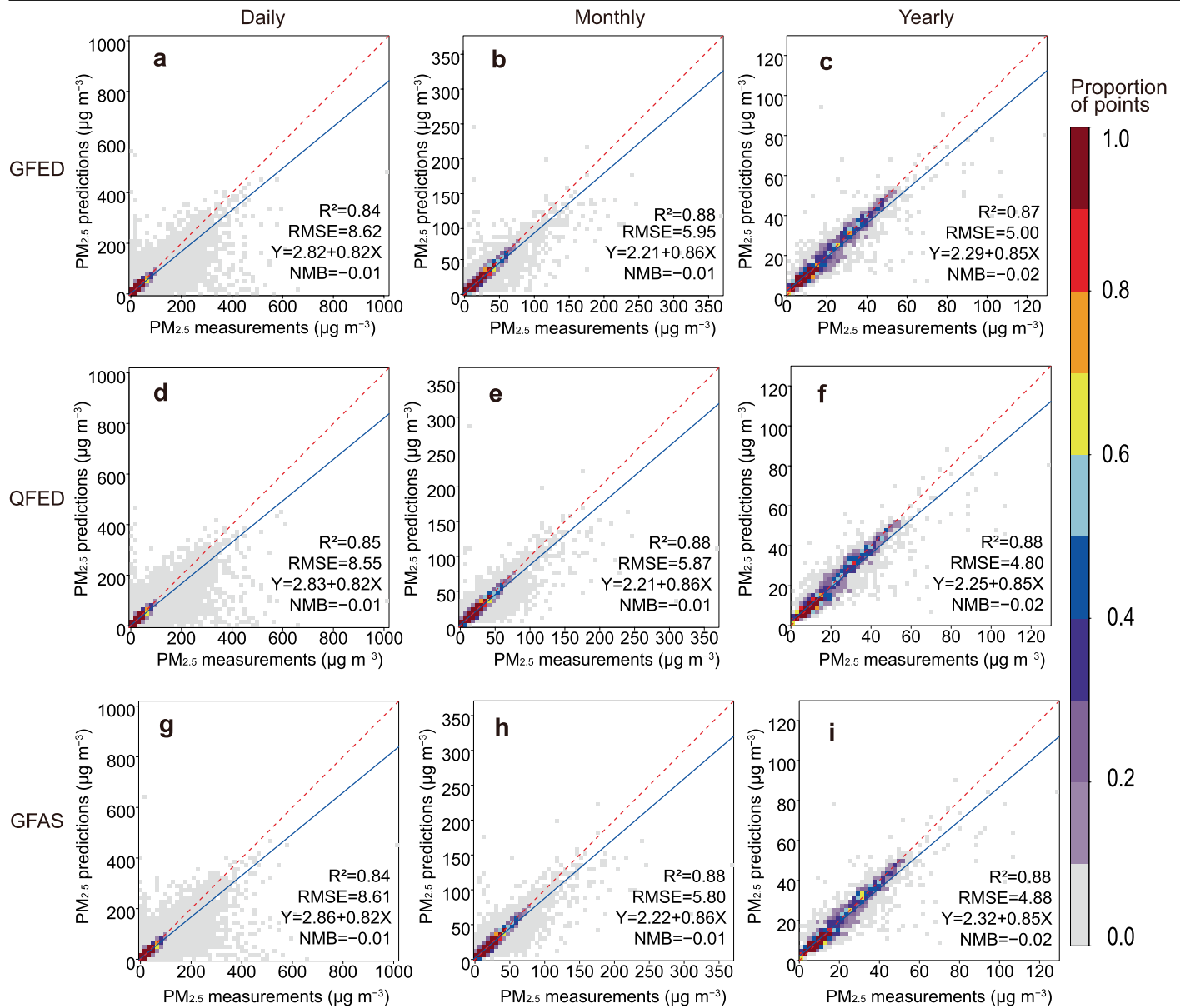




Extended Data Fig. 6 | Spatial distribution of annual primary PM_{2.5} emissions from wildfires over North America in 2023 in different emission inventories. a, in GFEDv4.1s. b, in QFEDv2.5r1. c, in GFASv1.2.

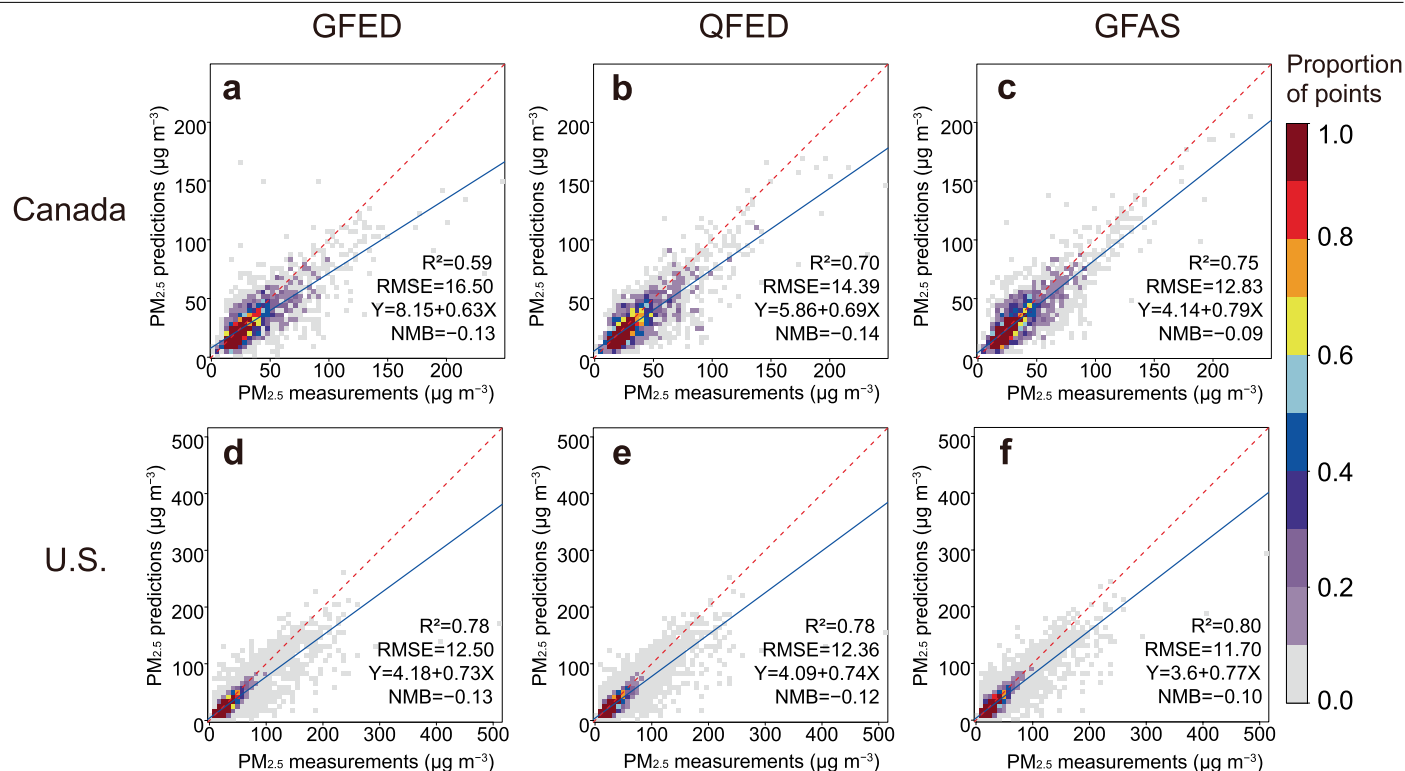


Extended Data Fig. 7 | The cumulative population PM_{2.5} exposure in the U.S. in 2023 attributable to different wild fire source regions. The colors of the dash lines denote Canadian fires, U.S. fires and other fires.



Extended Data Fig. 8 | Station-based cross-validation performance for estimating all-source $PM_{2.5}$ concentrations. **a,b,c**, Station-based twenty-fold cross-validation results for estimating all-source $PM_{2.5}$ using GFED as *a priori* fire emission at daily (**a**), monthly (**b**), and yearly (**c**) scale in the year 2023, respectively. RMSE, root mean squared error. NMB, normalized mean bias. **d,e,f**, Station-based twenty-fold cross-validation results for estimating all-source $PM_{2.5}$ using QFED as *a priori* fire emission at daily (**d**), monthly (**e**), and yearly (**f**) scale in the year 2023, respectively. **g,h,i**, Station-based twenty-fold cross-validation results for estimating all-source $PM_{2.5}$ using GFAS as *a priori* fire emission at daily (**g**), monthly (**h**), and yearly (**i**) scale in the year 2023, respectively. Ground-based $PM_{2.5}$ measurements collected globally, including

data from North America (Environmental Canada: <https://data-donnees.az.ec.gc.ca/data/air/monitor/national-air-pollution-surveillance-naps-program/Data-Donnees/>, US Environmental Protection Agency: <https://www.epa.gov/outdoor-air-quality-data/download-daily-data>, Interagency Monitoring of Protected Visual Environments: <https://views.cira.colostate.edu/fed/QueryWizard/Default.aspx>, and AirFire program of the US Forest Service: <https://info.airfire.org/airmonitor-package>), Europe (European Air Quality Portal: <https://eeadmz1-cws-wp-air02.azurewebsites.net/>), China (China National Environmental Monitoring Center: <http://www.cnemc.cn/>), and other regions (OpenAQ: <https://openaq.org/>).



Extended Data Fig. 9 | Cross-validation performance for estimating $PM_{2.5}$ during fire events. **a,b,c**, Twenty-fold cross-validation results for estimating $PM_{2.5}$ during fire events over Canada using GFED (**a**), QFED (**b**) and GFAS (**c**) as *a priori* fire emission in the year 2023. RMSE, root mean squared error.

NMB, normalized mean bias. **d,e,f**, Twenty-fold cross-validation results for estimating $PM_{2.5}$ during fire events over U.S. using GFED (**d**), QFED (**e**) and GFAS (**f**) as *a priori* fire emission in the year 2023.

Extended Data Table 1 | Annual mean PM_{2.5} exposure attributable to different sources in 2023 and acute exposure metrics of 2023 Canadian wildfires in global regions

Region	PM _{2.5} exposure (µg m ⁻³)							Acute exposure metrics		
	All	Anthropogenic	Other	Total fires	Canadian fires	U.S. fires	Other fires	Annual total person-days (billion)	Annual average days per person	Annual total number of exposed people (million)
World	26.29	18.67	6.30	1.32	0.17	0.02	1.13	4.84	0.60	354
Asia	33.04	26.16	6.10	0.78	0.06	0.00	0.72	0.00	0.00	0.03
Europe	10.52	7.76	2.20	0.56	0.41	0.01	0.14	0.05	0.07	47.7
Middle East and North Africa	23.77	14.03	9.37	0.38	0.22	0.01	0.14	0.00	0.00	0.83
North America	10.69	6.65	2.20	1.85	1.08	0.21	0.55	4.79	7.93	306
Canada	9.67	4.81	0.84	4.02	3.82	0.13	0.07	1.10	27.1	38.1
U.S.	8.65	5.10	1.59	1.96	1.49	0.35	0.12	3.69	11.0	267
Oceania	10.42	3.38	6.15	0.90	0.00	0.00	0.90	0.00	0.00	0.00
South America	14.88	8.44	4.92	1.52	0.00	0.00	1.52	0.00	0.00	0.00
Sub-Saharan Africa	24.56	9.89	10.75	3.92	0.02	0.00	3.89	0.00	0.00	0.00

Definitions of global regions are presented in Extended Data Fig. 3a.